

Late Cenozoic tectonic evolution of the southern Chinese Tian Shan

A. Yin, S. Nie,¹ P. Craig,² and T. M. Harrison

Department of Earth and Space Sciences and Institute of Geophysics and Planetary Physics
University of California, Los Angeles

F. J. Ryerson

Institute of Geophysics and Planetary Physics, Lawrence Livermore National Laboratory, Livermore, California

Qian Xianglin and Yang Geng

Department of Geology, Peking University, Beijing

Abstract. Structural, sedimentological, magnetostratigraphic, and ⁴⁰Ar/³⁹Ar thermochronological investigations were conducted in the southern Chinese Tian Shan. On the basis of our own mapping and earlier investigations in the area, the Late Cenozoic southern Tian Shan thrust belt may be divided into four segments based on their style of deformation. From west to east, they are (1) Kashi-Aksu imbricate thrust system, (2) the Baicheng-Kuche fold and thrust system, (3) the Korla right-slip transfer system, and (4) the Lop-Nor thrust system. The westernmost Kashi-Aksu system is characterized by the occurrence of evenly spaced (12-15 km) imbricate thrusts. The Baicheng-Kuche and Korla systems are expressed by a major north dipping thrust (the Kuche thrust) that changes its strike eastward to become a NW striking oblique thrust ramp (the Korla transfer zone). The Lop Nor system in the easternmost part of the southern Chinese Tian Shan consists of widely spaced thrusts, all involved with basement rocks. Geologic mapping and cross-section construction suggest that at least 20-40 km of crustal shortening with a horizontal shortening strain of 20-30% has occurred in the southern Chinese Tian Shan during the late Cenozoic. These estimates are minimum because of both conservative extrapolation of the thrust geometries and partial coverage of the thrust belt by the cross sections. The timing of initial thrusting is best constrained in the Kuche basin where crustal shortening may have occurred at 21-24 Ma, the time of a major facies transition between lacustrine and braided-fluvial sequences constrained in general by biostratigraphy and in detail by magnetostratigraphy. This estimate represents only a minimum age, as development of thrusts in the southern Chinese Tian Shan may have propagated southward toward the foreland. Thus the sedimentary record only represents the southernmost and therefore youngest phase of thrusting. If our estimate of timing for the thrust initiation (21-24 Ma) is correct, using the estimated magnitude of shortening (20-40 km) and shortening strain (20-30%), the averaged rates of late Cenozoic horizontal slip and shortening strain are 1-1.9 mm yr⁻¹ and 2.9-4.5x10⁻¹⁶ s⁻¹, respectively. Our reconnaissance ⁴⁰Ar/³⁹Ar thermochronological analysis in conjunction with earlier published results of apatite fission

track analysis by other workers in the Chinese Tian Shan suggests that the magnitude of Cenozoic denudation is no more than 10 km, most likely less than 5 km. We demonstrate via a simple Airy-isostasy model that when the thermal effect on changes in surface elevation is negligible, determination of the spatial distribution and temporal variation of both horizontal shortening strain and denudation becomes a key to reconstructing the elevation history of the Tian Shan. Using this simple model, the loosely constrained magnitude of crustal-shortening strain and denudation in the southern Chinese Tian Shan implies that it may have been elevated 1.0-2.0 km since the onset of Cenozoic thrusting.

1. Introduction

Intracontinental deformation which has occurred over a broad area of Asia during the late Cenozoic has been attributed to the collision of India with Asia, deforming southern Asia for as much as 2000-2500 km northward [Molnar and Tapponnier, 1975]. The relationship between the northward movement of India and corresponding strain partitioning within Asia is of mounting interest among geologists worldwide. One debate emerging from this renewed focus is whether crustal thickening or lateral extrusion has been the dominant mechanism for accommodating the convergence [Molnar and Tapponnier, 1975; England and Houseman, 1988; Dewey and Burke, 1973; Tapponnier et al., 1982; Peltzer and Tapponnier, 1988; Harrison et al., 1992a] and how the Cenozoic deformation in Asia has propagated from the Indus-Yalu suture northward where the collision initiated [e.g., Burchfiel and Royden, 1991; Harrison et al., 1992a]. The results of recent geologic investigations in and around the Tibetan plateau suggest that the deformation history of Asia due to collision may not be simply explained by one of the two mechanisms [Tapponnier et al., 1990; Harrison et al., 1992b; Burchfiel et al., 1991; Zhang et al., 1991; Burchfiel and Royden, 1991; Amano and Taira, 1992]. Rather, Cenozoic deformation styles in Asia may have varied during the collision as indicated by multistage deformation histories with a variety of regimes and distributions. For example, geologic mapping along the northern edge of the Tibetan plateau suggests that the deformation did not begin in this region until near the end of the Pliocene [Burchfiel et al., 1991; Zhang et al., 1991]. Apatite fission track analysis suggests rapid cooling occurred at about 20-25 Ma in the Tian Shan and western Kunlun Shan, which may be attributed to the tectonically induced uplift in the region

¹Now at Petroconsultants, Geneva, Switzerland.

²Now at Shell Deepwater Production, Inc., New Orleans, Louisiana.

[Hendrix *et al.*, 1994; Sobel, 1995; Sobel and Dumitru, 1997]. Studies on the Red River fault in southeastern China [Tapponnier *et al.*, 1990; Harrison *et al.*, 1992b; Leloup *et al.*, 1993] show that the fault changed from left slip to right slip between 17 and 5 Ma. In addition, the Gangdese thrust system in southern Tibet began to develop in the early Miocene at about 27 Ma [Yin *et al.*, 1994], some 30 m.y. after the initial collision of India and Asia [Burbank *et al.*, 1996]. Despite these efforts, there remain few constraints on timing and magnitude of late Cenozoic deformation in the central Tibetan plateau and the Tian Shan region to the north.

A key to understanding the Indo-Asian collision is to establish the spatial distribution and temporal variation of crustal strain in Asia. This, in turn, has important implications for paleotopographic and paleoclimatic histories of Tibet and its adjacent regions. It has been suggested that the Cenozoic topography of Asia, notably the Tibetan plateau, may have played an important role in global climate change [e.g., Ruddiman and Kutzback, 1989; Harrison *et al.*, 1992a; Molnar *et al.*, 1993]. Quantification of the interplay between climate and tectonically created topography in Asia requires knowledge of timing and magnitude of lithospheric deformation, history of surface

erosion and tectonic denudation, and records of chronological changes of climate. To address these issues, an integrated investigation of structural geology, sedimentology, magnetostratigraphy, and $^{40}\text{Ar}/^{39}\text{Ar}$ thermochronology was conducted in the southern Chinese Tian Shan, northwestern China (Figures 1 and 2). Specifically, we address the questions of when Cenozoic deformation initiated, how much crustal deformation occurred in the southern Chinese Tian Shan since the beginning of the Indo-Asian collision, and what was the elevation history of the Tian Shan during the Cenozoic. This paper provides a geologic synthesis of the southern Chinese Tian Shan region based on both our own investigations and previously published work in the region. Most place names in the paper follow the spelling of Chinese pinyin. However, those that are well known to westerners such as Hotan, Kuche, and Tarim will retain their conventional spelling as commonly shown on western maps.

2. Regional Tectonics

The Tian Shan extends broadly east-west for over 2500 km across central Asia (Figure 1) with peaks exceeding 7000 m and

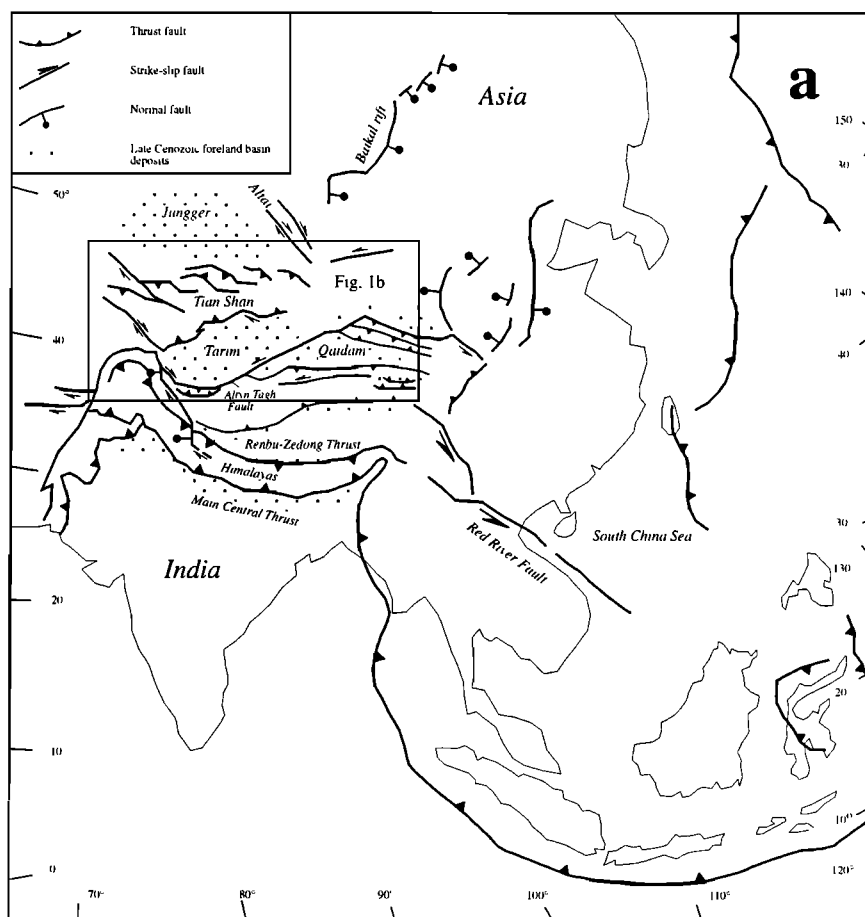


Figure 1. (a) Tectonic map of Indo-Asian collisional system. (b) Simplified Cenozoic tectonic map of central Asia and location of Tian Shan (modified after Peltzer and Tapponnier [1988]). Abbreviations are as follows: ATF, Altyn Tagh fault; KF, Karakorum fault; Ka, Kashi; H, Hotan; Ku, Kuche; and Ko, Korla. Contours show thickness distribution of Cenozoic sediments in Tarim based on Li *et al.* [1996]. Note that there are two depositional centers: one near Kuche (Kuche foreland basin) and one near Hotan (Hotan foreland basin). (b) Simplified geologic map of Chinese Tian Shan after Chen [1985] with our own observations and interpretation. Locations of Figure 2 and $^{40}\text{Ar}/^{39}\text{Ar}$ samples are shown.

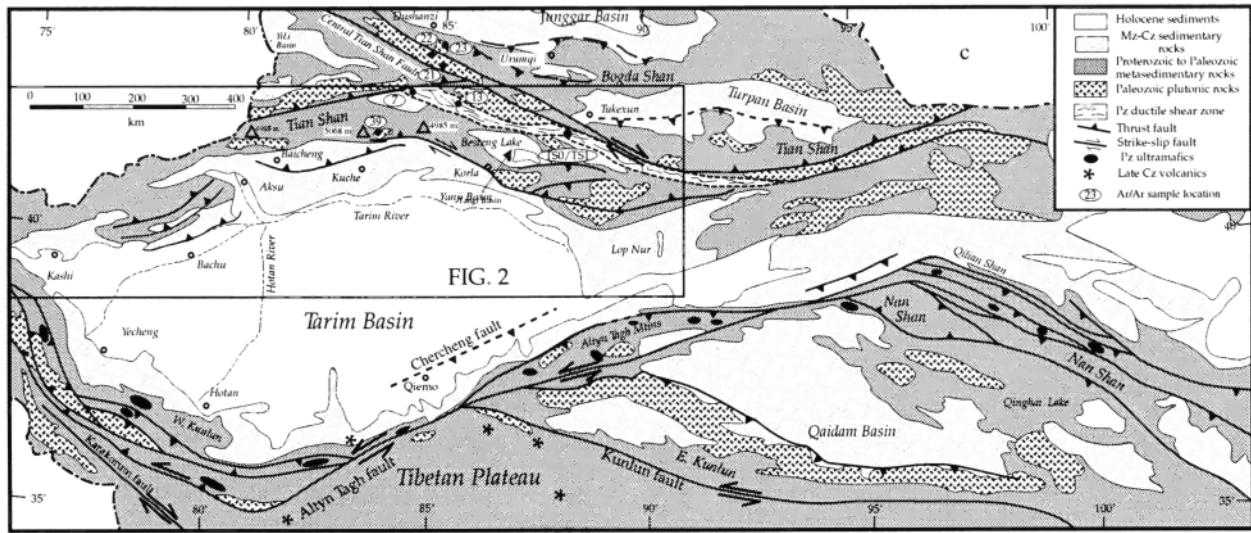
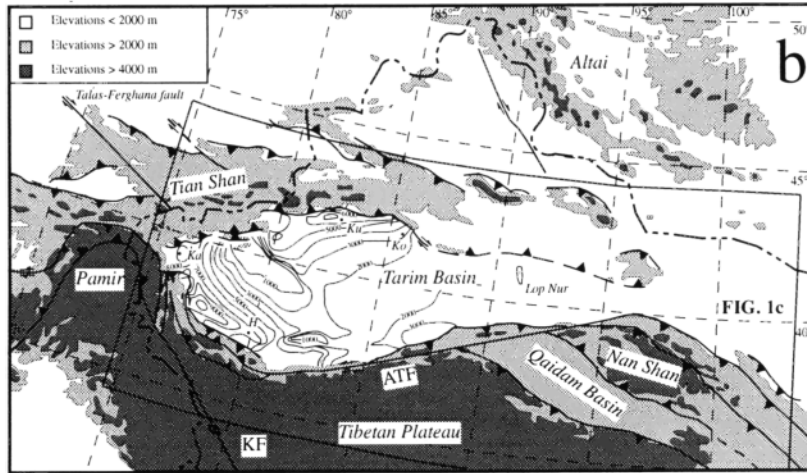


Figure 1. (continued)

with basins lower than 100 m below the sea level. The Tian Shan merges with the E-W trending Qilian Shan and NW-trending Altai Shan to the east and the Pamir syntaxis to the west (Figure 1). The thrust system in Pamir links with the

western Kunlun thrust belt on the southeast side of the Tarim basin. It, in turn, links with the western termination of the Altyn Tagh fault system that bounds the southwest side of the Tarim basin (Figure 1) [Avouac and Peltzer, 1993]. The thrusts

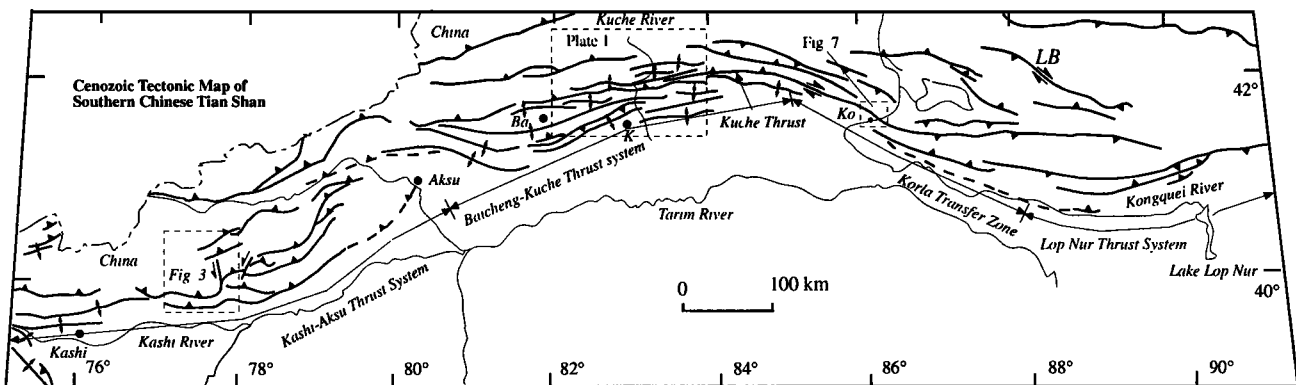


Figure 2. Simplified tectonic map of southern Chinese Tian Shan thrust belt (modified from Chen [1985]). The belt is divided into four segments: (1) the Kashi-Aksu thrust system, (2) the Baicheng-Kuche thrust system, (3) the Korla transfer fault zone, and (4) the Lop Nur thrust system. Locations of Figures 3 and 7 and Plate 1 are shown.

in the Pamir and the western Kunlun Shan accommodate the southward subduction of the Tarim block [Lyon-Caen and Molnar, 1984], producing seismicity at depths greater than 100 km [Burtman and Molnar, 1993].

Geologic reconnaissance of the Chinese Tian Shan was first conducted by Norin [1941] during a 4-year Sino-Swedish expedition. His work emphasized both lithostratigraphy and biostratigraphy, which formed the foundation for subsequent stratigraphic studies in the region. Following his pioneering work, later studies revealed that the Chinese Tian Shan has experienced multiple phases of deformation [e.g., Xinjiang Institute of Geography, Academia Sinica, 1986; Xinjiang Bureau of Geology and Mineral Resources (Xinjiang BGM), 1992; Jia et al., 1991; Hendrix et al., 1992; Zhou and Zheng, 1990]. Huang [1945] was perhaps the first who noted that the Chinese Tian Shan region has experienced multiple episodes of deformation. In recent years, the multiphased deformation in the Tian Shan region has been interpreted in the context of plate tectonics. A middle Paleozoic Tian Shan orogeny was suggested to have developed because of one or more arc-continental collisions [Coleman, 1989; Windley et al., 1990; Allen et al., 1992; Carroll et al., 1995], followed by reactivation of the older faults caused by successive collision of island-arc systems onto the southern margin of Asia in the late Paleozoic and the Mesozoic [Hendrix et al., 1992; Sobel, 1995]. The region was again rejuvenated in the late Cenozoic because of the Indo-Asian collision [Tapponnier and Molnar, 1979; Burchfiel and Royden, 1991; Lu et al., 1994; Liu et al., 1994].

The present Tian Shan is flanked by east-west trending, active thrust systems on its north and south sides [Molnar and Tapponnier, 1975; Tapponnier and Molnar, 1979; Burchfiel and Royden, 1991; Avouac et al., 1993; Molnar et al., 1994; Burchfiel et al., 1994; Nie et al., 1994]. The axial part of the mountain range is transected by the WNW-trending central Tian Shan fault system of Hendrix et al. [1992], which links with a variety of late Cenozoic thrust systems (Figure 1). This fault system was recognized from Landsat images by Tapponnier and Molnar [1979] as an active right-slip fault. This fault bounds the intermontane basins in the Chinese Tian Shan such as the Turpan, Yili, and Yanji basins, and terminates at a thrust system near Lop Nor in the eastern Tian Shan (Figure 1).

The Tarim basin between the Tian Shan and the Tibetan plateau is mostly covered by Neogene and Quaternary sediments (Figure 1). Because of its economic importance, extensive drilling and seismic reflection studies have been conducted in the Tarim region [Zhou and Chen, 1990; Jia et al., 1991; Kang, 1996], which suggest that the basin has a protracted deformation history, similar to the Tian Shan [Jia et al., 1991; Hendrix et al., 1992; Carroll et al., 1995; Sobel, 1995; Li et al., 1996]. The seismic-reflection profiles suggest that central Tarim is underlain by a middle Paleozoic contractional belt [Jia et al., 1991]. Widespread marine sedimentation beginning in the Late Carboniferous occurred immediately after the collision in the Tian Shan and ended in the late Early Permian. In addition, widespread Triassic-Jurassic deformation has also been documented in the northeastern Tarim basin [Jia et al., 1991]. These structures are variably interpreted as contractional [Jia et al., 1991] or transpressional structures [Yan, 1991]. Northern Tarim was a foreland basin between Triassic and Early Cretaceous, which has unconformities and pulses of conglomerate deposition interpreted to record intervals of renewed Mesozoic compression and uplift of the Tian Shan [Hendrix et al., 1992]. A series of shallow marine transgressions, entering the Tarim basin from Tadjik basin to the west, occurred between the beginning of the Late Cretaceous and early Oligocene [Hao and Zeng, 1984]. During the transgressions, the Upper Cretaceous

through Lower Oligocene sediments were deposited in a shallow sea as indicated by alternating shallow marine and hypersaline lagoon to nonmarine units [Sobel, 1995]. The transgression in the Paleocene may have covered much of the Tarim basin, as indicated by the presence of thick Paleocene gypsum deposits [Sobel, 1995]. In the late Oligocene and early Miocene, most of the western and northern Tarim basin was covered by gypsum-bearing beds, which have been consistently interpreted by Chinese geologists as marine deposits (e.g., the late Oligocene Avate and early Miocene Suweiyi Formations in the Kuche region, and the late Oligocene Bashibulake Formation in the Kashi region [see Ye and Huang, 1990]. This includes the two Cenozoic depositional centers with sediments in excess of 5 km in thickness: the Kuche and the Hotan foreland basins [Li et al., 1996] (Figure 1). Their development has been related to thrusting in the Tian Shan and western Kunlun Shan [Li et al., 1996]. The presence of the late Oligocene marine sediments in the southern Chinese Tian Shan and western Kunlun Shan implies that (1) the two mountain ranges did not begin to uplift after the early Oligocene and (2) the southernmost Chinese Tian Shan has been uplifted for at least 1.5-2.0 km, which are the current elevations for these marine beds.

3. Southern Tian Shan Thrust Belt

The southern Tian Shan thrust belt may be divided into four segments based on their styles (e.g., basement involved versus thin skinned and lateral ramps versus frontal ramps) and struc-

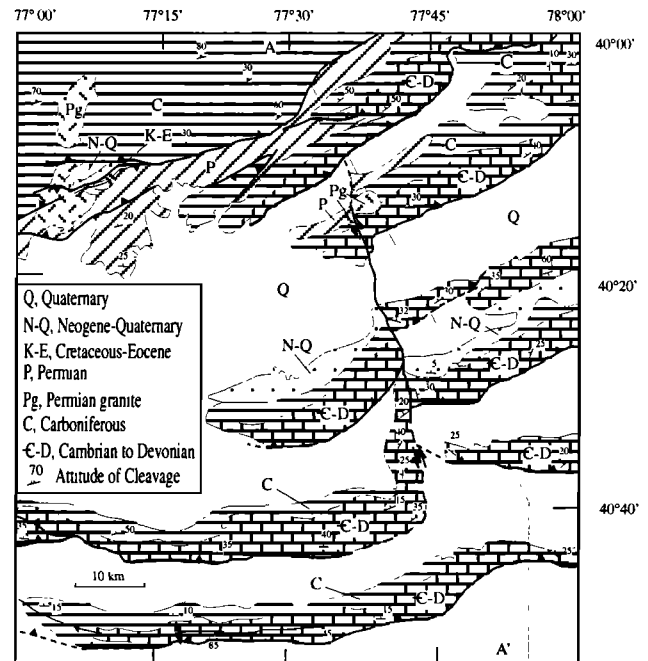


Figure 3. Geologic map of a part of the Kashi-Aksu thrust system, modified from Xinjiang BGM [1967] with our own observations and interpretations. Symbols for rock units: C, Carboniferous limestone; C-D, Cambrian dolomite and cherty limestone, Ordovician limestone, shale, and sandstone, Silurian sandstone, shale, and limestone, and Devonian red siltstone and sandstone; K-E, Cretaceous-Paleogene sandstones, claystone, and siltstone; N-Q, Neogene and Quaternary sandstones and conglomerate; Pg, Permian granite. AA' is the location of the cross section shown in Figure 4.

tural trend. From west to east (Figure 2), they are (1) the Kashi-Aksu thrust system, (2) the Baicheng-Kuche thrust system, (3) the Korla transfer system, and (4) the Lop Nor thrust system. Of the four segments, we studied portions of the Baicheng-Kuche thrust system and the Korla transfer system in detail. Description of the Kashi-Aksu and Lop Nor thrust systems are mainly based on the existing Chinese geologic maps at scales of 1:200,000 and 1:1,000,000 [Xinjiang BGM, 1965a, b, 1966a, b, c, 1967, 1975], regional geologic reports [Xinjiang BGM, 1992], a structural investigation by McKnight [1993] on the Kashi-Aksu thrust belt, and our own reconnaissance observations.

3.1. Kashi-Aksu Thrust System

The Kashi-Aksu thrust system (Figures 2 and 3), also known as the Kalpin uplift, was first systematically mapped in 1955 and 1956 by Chinese and former USSR geologists, which resulted in 1:200,000-scale geologic maps [Xinjiang BGM, 1965a, 1966a, b, 1975]. The general structural style and magnitude of shortening across the region were recently reevaluated by McKnight [1993, 1994] on the basis of Landsat images and field studies.

The Kashi-Aksu thrust system consists of thrust imbricates involving strata from Cambrian to Quaternary (Figure 3 and cross section AA' in Figure 4). McKnight [1993, 1994] was the first to recognize the thin-skin style of thrusting in this thrust system. He projects the decollement to the base of the Cambrian strata, which are the oldest exposed unit in the imbricate system. In the northern part of the thrust system, deformation involves the Devonian and Carboniferous strata and is characterized by isoclinal folding. The angular unconformity between the Carboniferous and the folded strata below [Chen, 1985] implies significant crustal deformation during the middle Paleozoic. This regional unconformity is attributed to complex collisional processes first between Tarim and south Tian Shan followed by collision between north and south Tian Shan [Carroll et al., 1995]. The thickness of the upper Paleozoic strata in the Kashi-Kuche thrust system increases from south to north. The Paleozoic strata in the thrust system thicken from about 2 km in the south to greater than 4 km in the north [Xinjiang BGM, 1965a; Carroll et al., 1995].

The stratigraphic configuration determines the style of deformation and the spacing of the thrusts. In the southern part of the thrust system, where the thickness of the Paleozoic strata is relatively thin, all the imbricate thrust sheets share

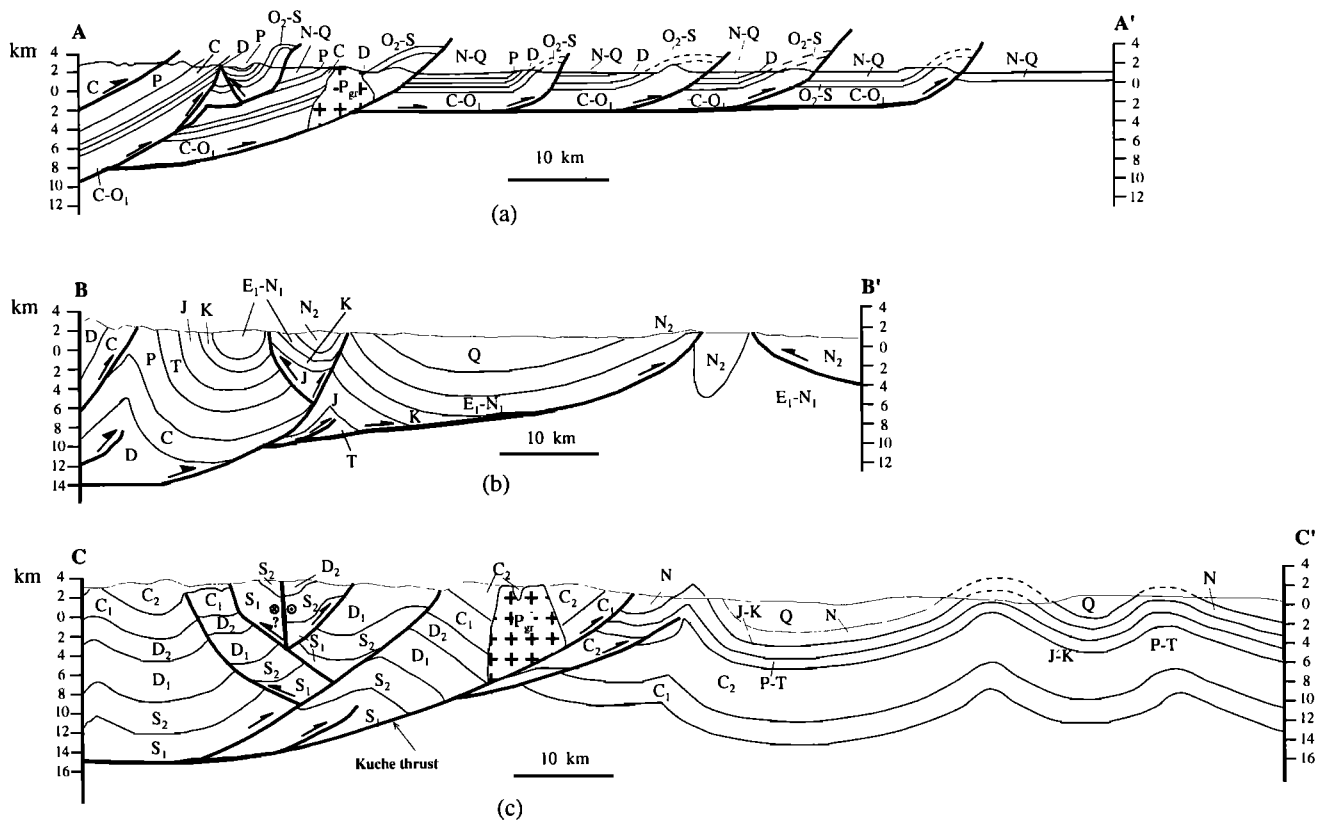


Figure 4. Geologic cross sections (a) AA' through the Kashi-Aksu thrust system, (b) BB' through the western part of the Baicheng-Kuche thrust system, and (c) CC' through the eastern part of the Baicheng-Kuche thrust system. See Figure 3 and Plate 1 for location. In cross section AA', abbreviations are as follows: C-O₂, Cambrian to lower Ordovician; O₂-S, middle Ordovician to Silurian; D, Devonian; C, Carboniferous; P, Permian; and N-Q, Neogene to Quaternary. In cross section BB', abbreviations are as follows: D, Devonian; C, Carboniferous; P, Permian; T, Triassic; J, Jurassic; K, Cretaceous; E₁-N₁, Paleogene to lower Miocene; N₂, middle Miocene to Pleistocene; and Q, Quaternary. In cross section CC', abbreviations are as follows: S₁, Lower Silurian; S₂, Middle Silurian; D₁, Lower Devonian; D₂, Upper Devonian; C₁, Lower Carboniferous; C₂, Upper Carboniferous; Pg, Permian granite; P-T, Permian to Triassic; J-K, Jurassic to Cretaceous; N, Neogene; and Q, Quaternary.

the same basal unit, an Upper Cambrian limestone. This implies the presence of a decollement at this stratigraphic interval as inferred by *McKnight* [1993]. The spacing of the thrusts in the southern part of the thrust belt is remarkably consistent at about ~12-15 km, suggesting a constant thickness of the Paleozoic units above the decollement, consistent with the observed thickness of the Paleozoic strata in the field [*Xinjiang BGM*, 1965a]. It also implies that the initiation of the thrusts was induced by folding instability [*Smith*, 1977], as it produces a spatial periodicity of stress concentration. In contrast to the southern part of the thrust system, the thickness of the Paleozoic strata is both greater and more variable in the northern thrust system. As a result, the thrusts are more closely spaced, folds are tighter, and back thrusts are well developed.

Because the hanging wall cutoffs of the imbricate thrusts have been eroded away, it is difficult to estimate the exact amount of shortening across the thrust system. However, by projecting stratigraphic contacts and fault trajectories, the minimum amount of Cenozoic shortening across the thrust system was estimated to be 23 km, which implies 22% shortening strain. This estimate was based on the interpretation that the basal decollement follows the same stratigraphic unit and steepens northward as a result of increase in thickness of the Carboniferous-Permian strata (cross section AA' in Figure 4). This estimate is a minimum, because hanging wall units are extrapolated as simple hanging wall anticlines against the upward projection of the thrust faults. In a different approach, *McKnight* [1993] assumes a fault-bend fold geometry for the hanging wall strata of individual thrusts. Under this assumption, the hanging wall cutoffs are projected much farther in the thrust transport direction. Consequently, 50 km of Cenozoic shortening across the thrust system was estimated, significantly greater than our estimate. As the projected fault-bend folds above the thrusts have been eroded away, it is difficult to test the validity of this model.

3.2. Baicheng-Kuche Thrust System

The Baicheng-Kuche thrust system is characterized by a major north dipping thrust, the Kuche thrust, in its eastern part (Figure 2 and Plate 1). This thrust connects with the Korla transfer system to the east and numerous folds and minor thrusts to the west. The folds and thrusts in the western part of the system mark the termination of the Kuche thrust. The lack of evenly spaced imbricate thrusts in the Baicheng-Kuche thrust system contrasts sharply to the Kashi-Aksu thrust system. This may be attributed to the fact that the thickness of the Paleozoic-Mesozoic strata is significantly greater in the Baicheng-Kuche area (>10 km [see *Jia et al.*, 1991]) than that in the Kashi-Aksu system (~2.0 km), which prevents the occurrence of folding instability [*Smith*, 1977]. Instead, the competing process of fracturing occurred, resulting in the initiation and development of the Kuche thrust. The difference in style of deformation between the Kashi-Aksu and Baicheng-Kuche thrust systems was also noted by *McKnight* [1993]. He attributed it to differences in mechanical behavior between thick Paleozoic carbonate in the Kashi-Aksu system and relatively unconsolidated Cenozoic sediments in the Kuche foredeep.

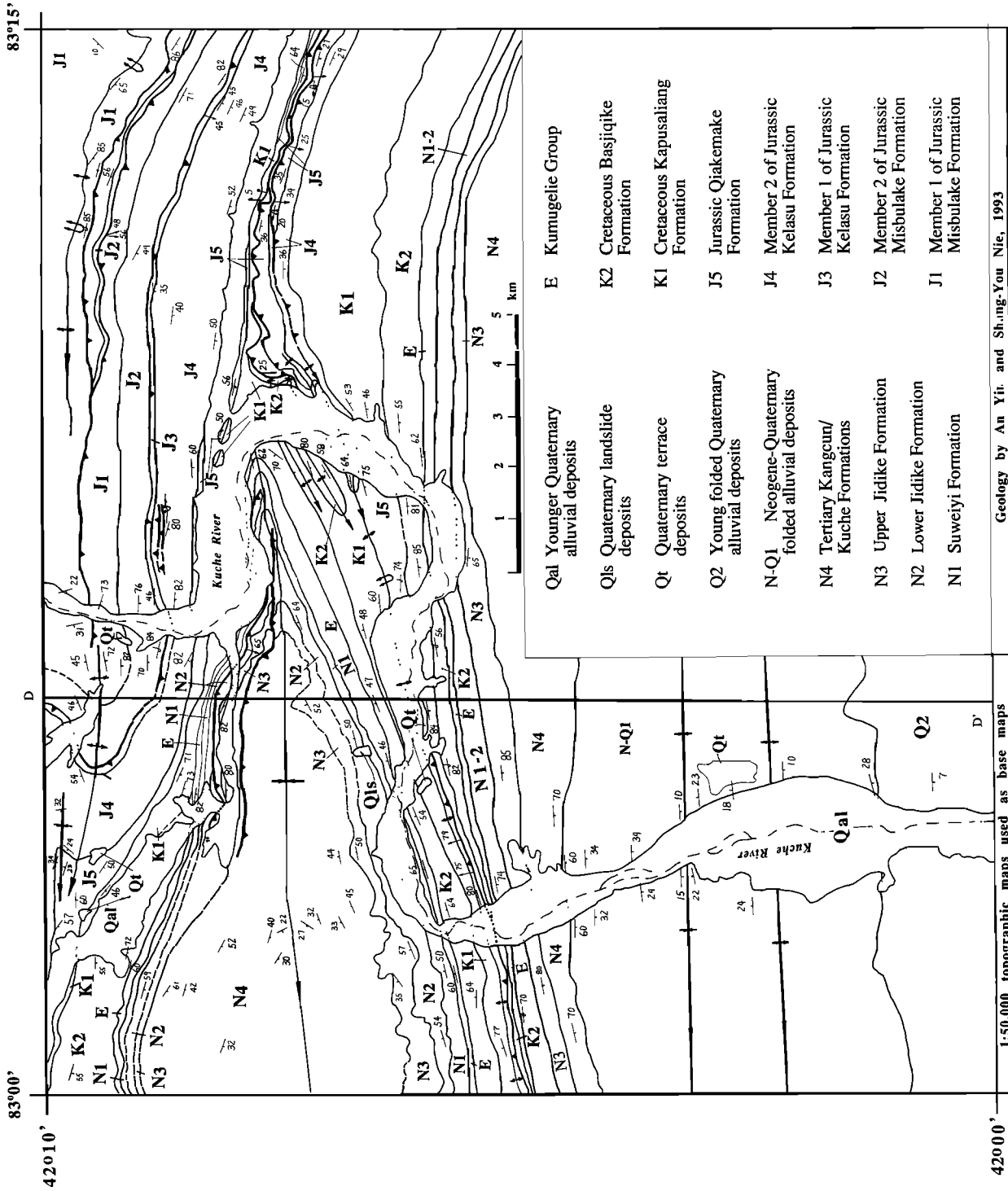
A sequence of Cenozoic sediments is exposed in the Kuche region, which decreases in thickness westward toward the Kashi-Aksu thrust system, eastward toward the Korla transfer fault system, and southward toward central Tarim (Figure 1). The westward decrease in stratigraphic thickness may be the result of protrusion of the Kashi-Aksu thrust system into the Tarim basin, which may have formed a structural high in the

Cenozoic, buttressing the western end of the Baicheng-Kuche thrust system. The eastward decrease in stratigraphic thickness corresponds spatially to the change in strike of the Kuche thrust from N80°E to N45°W (Figure 2), which may be related to the transition from thrusting to strike-slip faulting as the Kuche thrust changes its strike.

The Kuche thrust juxtaposes Carboniferous strata over Neogene-Quaternary sediments (Figures 5 and 6a). It dies into a broad anticline westward as its magnitude of slip decreases (Figures 5 and 6b). There are numerous north verging folds and north directed thrusts in the forelimb of the south verging anticline that terminates the Kuche thrust (Plate 1 and Figure 5). Several large thrusts and folds with unknown ages are present in the Lower Devonian strata of the hanging wall of the Kuche thrust. Associated with these structures are mesoscopic isoclinal folds (Figure 6c), which are significantly different in deformation style from that in the Mesozoic and Cenozoic strata isoclinal folds. In addition, a right-slip shear zone several tens of meters thick, which is characterized by the presence of foliated and lineated schist, is observed in the northern part of the study area in the Devonian strata (Plate 1). We speculate that both the ductile shear zone and isoclinal folds in the northern part of the study area are Paleozoic structures, although no solid evidence has been found in the field to constrain their ages.

A bedding-parallel thrust is present in the Upper Jurassic coal-bearing beds (Figures 5 and 6). This fault is presently folded by the south verging anticline which terminates the Kuche thrust. Minor south directed imbricate thrusts and south verging folds are present in places above this bedding-parallel fault, suggesting that the fault is south directed. Whether this bedding-parallel fault is a part of a flat-ramp thrust surface, a common thrust geometry in thrust belts [e.g., *Yin and Oertel*, 1993], with significant displacement is not clear. However, caution should be taken when interpreting stratigraphic sections and their sedimentologic evolution. Folded thrusts in Cenozoic strata have been reported in the northern Chinese Tian Shan by *Avouac et al.* [1993].

Folds in the Jurassic and older strata are generally open, whereas in the Cretaceous and Cenozoic strata they are generally tight and locally isoclinal (Plate 1 and Figure 5). The contrast in the tightness of folds implies that there may exist a bedding-parallel detachment at the base of the Upper Cretaceous strata, which is typically mudstone with minor fine-grained sandstone. Although there are minor back thrusts developed in the gypsum-rich beds of the lower Tertiary section (Figure 5), no evidence of major detachment faulting at this stratigraphic interval was observed. The amount of shortening is ~22 km in section BB' and ~42 km in section CC' (Figure 4). This suggests that the shortening strain is between 22% and 30% in the Baicheng-Kuche thrust system. In a similar attempt, *McKnight* [1993] estimated that the thin-skin portion of the Kuche thrust belt accommodated 10-30 km of shortening, whereas the thrusts within the interior of the southern Tian Shan has accommodated about 20 km shortening of the Cenozoic. Our estimates are broadly compatible with those of *McKnight* [1993]. In recent years, several cross sections have been constructed for the southernmost part of the Kuche thrust system, which is mostly covered by Quaternary deposits in the Tarim basin, based on seismic-reflection profiles [*Lu et al.*, 1994; *Liu et al.*, 1994]. These cross sections imply that additional 15-20 km of N-S shortening has occurred in the southern Tian Shan thrust belt. Because the locations of these cross sections are uncertain (i.e., no longitudes and latitudes are labeled in the index maps), we are unable to project the structures we depict based on surface mapping to those based on subsurface data.



a)

Figure 5

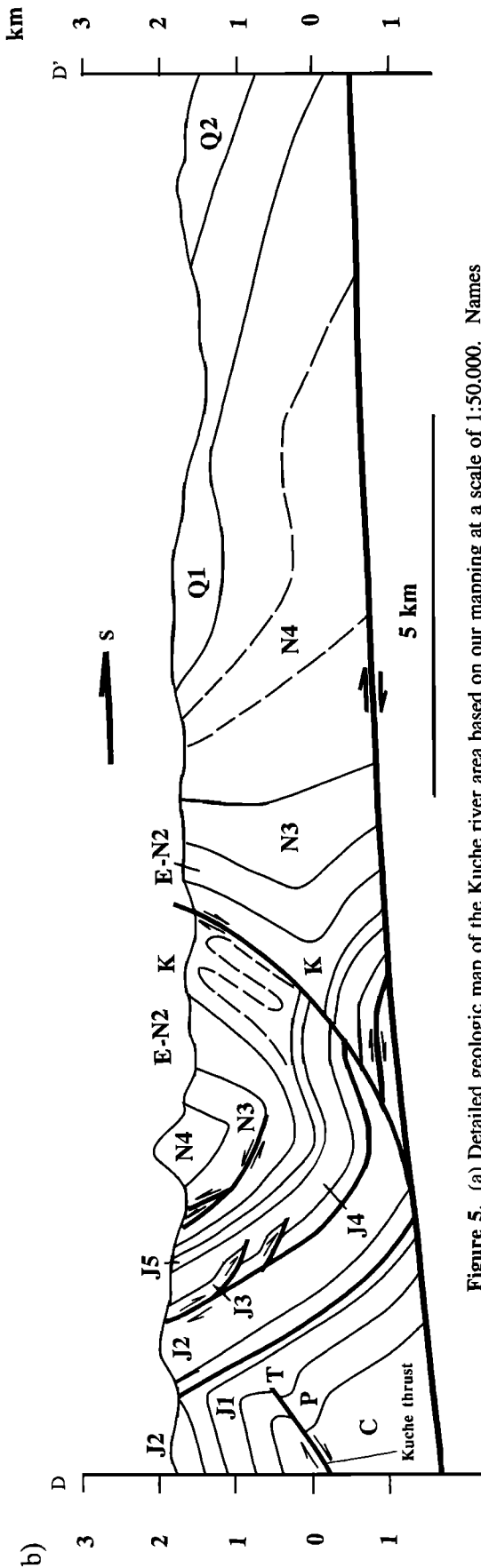


Figure 5. (a) Detailed geologic map of the Kuche river area based on our mapping at a scale of 1:50,000. Names of major stratigraphic formations follow those in the geologic map of the Kule region [Xinjiang BGM, 1975]. Many of those formations are further divided into subunits during our mapping for depicting detailed thrust and fold geometries. (b) Geologic cross section (DD') showing relationship between the Kuche thrust and folds (see Figure 5a for location). Note that a bedding-parallel, south-directed thrust in the Jurassic strata is folded.

3.3. Korla Transfer System

The Kuche thrust changes its strike abruptly from an E-W direction to a NW direction (Figure 2). Corresponding to the change is a drastic decrease in thickness of the Cenozoic sediments in the Kuche basin (Figure 1). The bending point of the Kuche fault marks the transition zone between the Baicheng-Kuche thrust system and the Korla transfer system. The Korla transfer zone links both the Baicheng-Kuche thrust system to the west and the thrusts north of the Korla fault (Figure 7). The Korla transfer system consists of both strike-slip and thrust faults. The thrusts are present in the northern part of the transfer system and bound the southern margin of the Yanji basin, whereas the strike-slip faults are exposed in the southern part of the transfer system and bound the northern margin of the Tarim basin (Figure 2). Near Korla, a thrust juxtaposes the Archean-Proterozoic metamorphic rocks over Jurassic coal-bearing strata (Figure 7). This fault is cut by a strike-slip fault in the Korla transfer zone and is unconformably overlain by Tertiary strata (Figure 7). The Tertiary strata are in turn folded with their axial traces trending in the east-west direction. Although kinematic data along the main strand of the strike-slip faults in the southern transfer zone are not available because of extensive Quaternary loess cover, numerous minor strike-slip faults adjacent to the inferred major strike-slip fault provide a clue as to its kinematics. We observed these minor faults in two places, one near Korla in the Jurassic section (Figure 6d) and one near the transition of the Baicheng-Kuche and the Korla fault system in the Carboniferous strata. In both places, minor strike-slip faults have a strike between $N45^{\circ}W$ and $N60^{\circ}W$ with subhorizontal striations on the fault surfaces. These minor faults are right-slip, as indicated by the offsets of lithologic units. The geometric relationship between the E-W trending Cenozoic folds and the Korla fault (Figure 7) also indicates that the sense of the strike-slip fault is right-lateral.

3.4. Lop Nor Transpressional System

Except for general information available from Xinjiang BGM [1992] and Chen [1985], little is known about the timing, kinematics, and magnitude of Cenozoic deformation in this part of the Chinese Tian Shan. The Lop Nor system is not only the eastern termination of the Korla transfer system (Figure 2), it also marks the eastern end of the central Tian Shan fault system (i.e., the central Tian Shan fault) in the eastern Tian Shan (Figure 1c). Although it cannot be directly estimated, the magnitude of shortening in this system appears smaller than that of the Baicheng-Kuche thrust system. If crustal shortening in the Baicheng-Kuche thrust system was completely transferred to the Lop Nor system through the Korla transfer zone, we would expect that thrusting in the Lop Nor area would have produced a similar magnitude of subsidence and sedimentation of the Cenozoic strata as observed in the Kuche basin. This is clearly not the case. One explanation for the discrepancy is that the shortening was only partially transferred to the Lop Nor thrust system because of slip partitioning by the thrusts bounding the Yanji basin (Figure 1c). Alternatively, the total amount of shortening in the Tian Shan region decreases from west to east as suggested by the eastward decrease in crustal thickness and topographic elevation [Avouac *et al.*, 1993]. Additionally, Burchfiel *et al.* [1994] suggested that the shortening in the Kashi-Aksu and the Baicheng-Kuche thrust systems was transferred to thrusts that bound the Bogda Shan in the northeastern Tian Shan (Figure 1c).

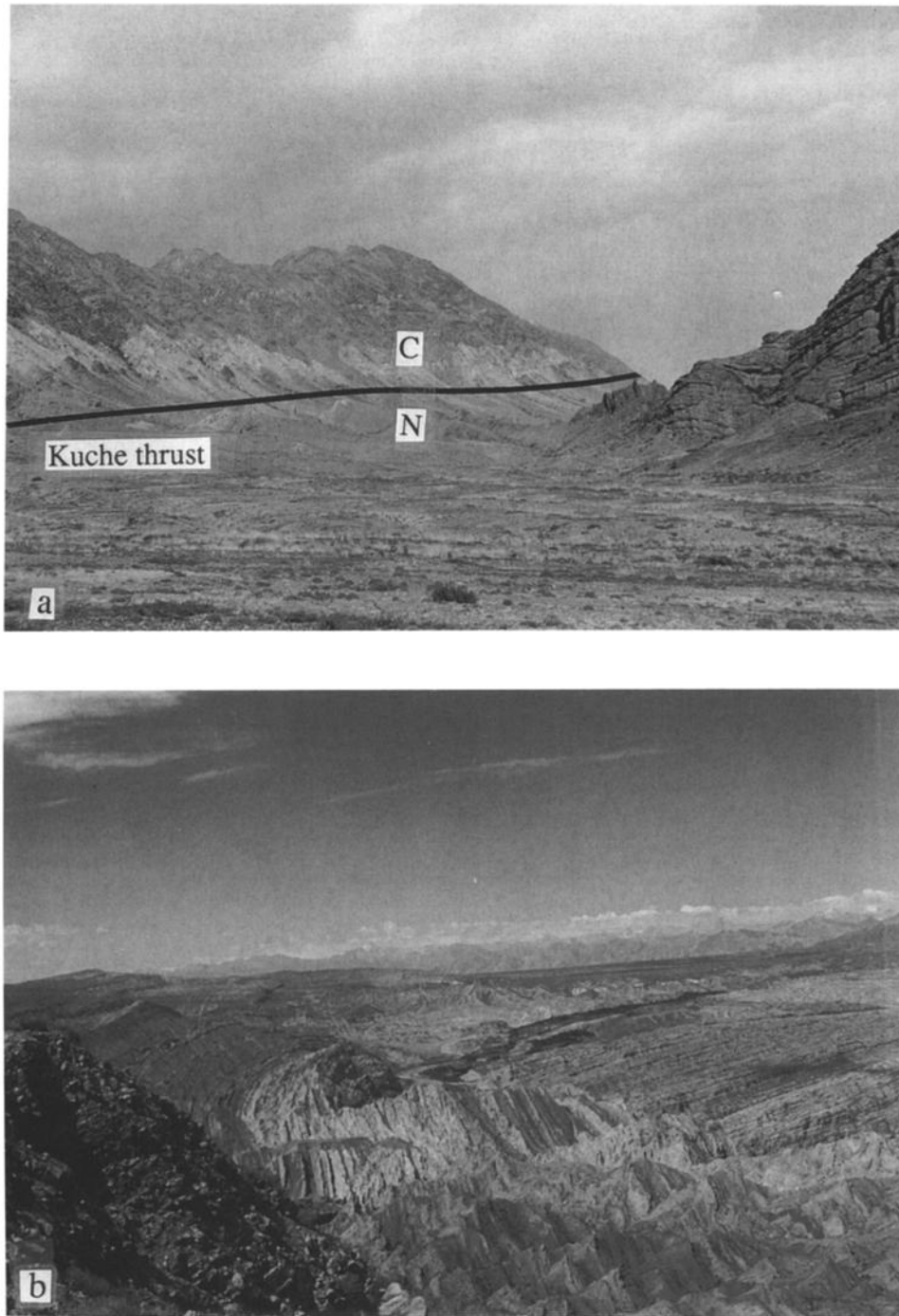


Figure 6. Pictures showing key field observations. (a) Kuche thrust juxtaposing Carboniferous strata (C) over Tertiary strata (N), view to the east. See Plate 1 for location. (b) A broad south-verging anticline, looking toward north. The Kuche thrust is inferred to be present beneath this anticline (cross section DD' in Figure 5b); see Plate 1 for location. (c) Isoclinal folds in cherty limestone of Lower Devonian strata. See Plate 1 for location. (d) Horizontal striations on a vertical fault in the Jurassic strata, looking toward north. The fault is NW striking and is part of the Korla transfer system; see Figure 7 for location.

4. Cenozoic Stratigraphy of the Kuche Basin

In order to determine the timing and rate of thrusting for the southern Chinese Tian Shan thrust belt, we examined the Cenozoic strata of the Kuche foreland basin, which is part of the

Tarim Basin and extends for approximately the length of the Baicheng-Kuche thrust system (Figure 1b). In this basin, the Cenozoic section is thick and well exposed. Because the chronology of our measured magnetostratigraphy is firmly based on the regional biostratigraphy established by Chinese

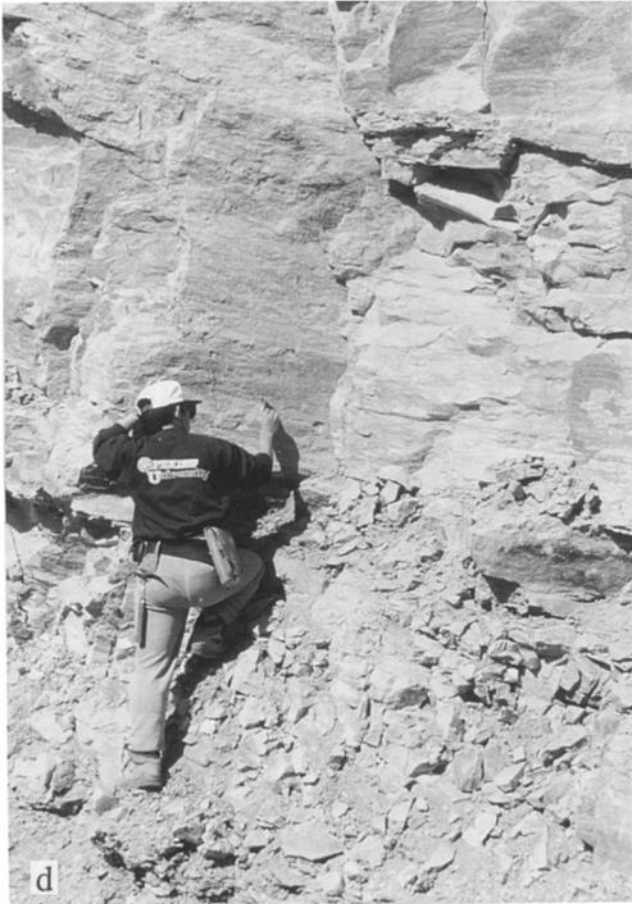
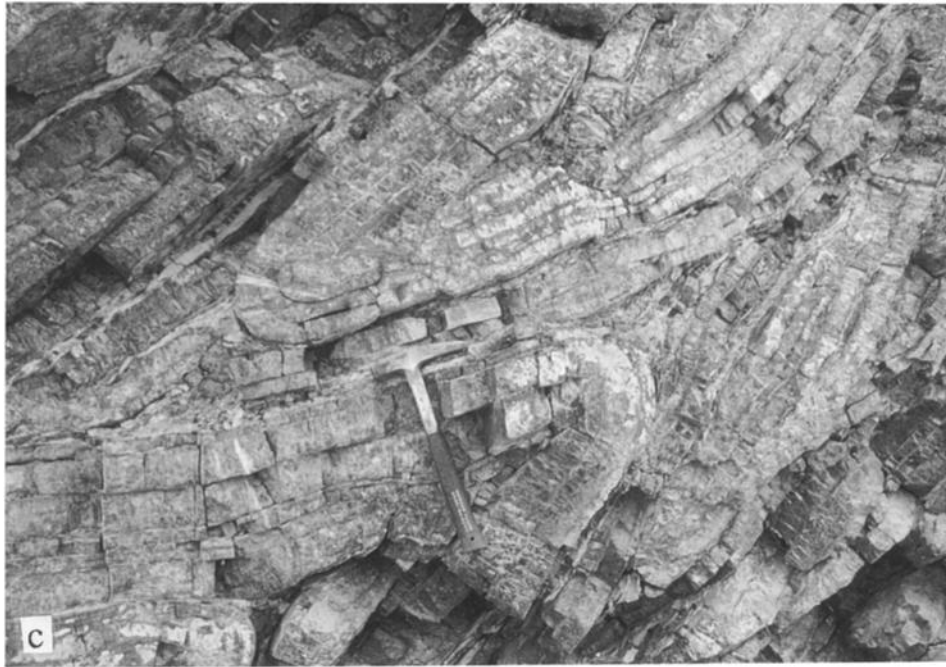


Figure 6. (continued)

geologists, we first summarize the available Cenozoic biostratigraphic data for the southern Chinese Tian Shan with special emphasis on the Kuche basin. We then present the results of our sedimentological and magnetostratigraphic investigations on two sections in the Kuche region.

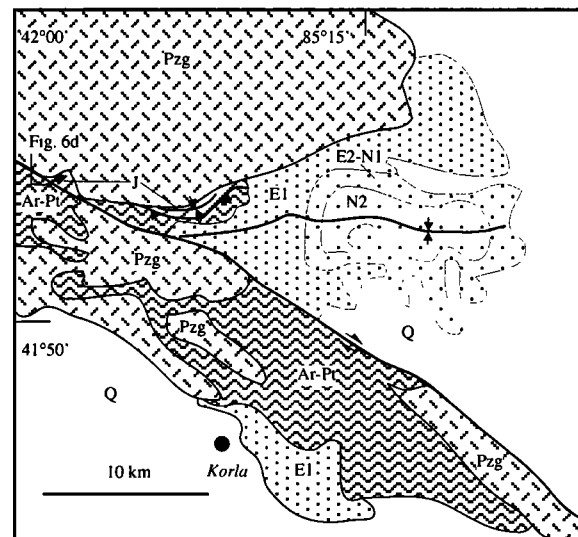


Figure 7. Geologic map of the Korla area. Abbreviations are as follows: Ar-Pt, Archean and Proterozoic metamorphic gneisses; Pzgr, Paleozoic granitoids; J-K, Jurassic and Cretaceous sedimentary rocks; E1, Paleocene mudstone and siltstone; E2-N2, Oligocene-early Miocene fine-grained to coarse grained sandstone; N2, upper Neogene coarse-grained sandstone and conglomerates; and Qal, Quaternary alluvial and lacustrine deposits.

4.1. Biostratigraphy

Late Cretaceous to early Tertiary biostratigraphy of the southern Tian Shan and northern Tarim basin are arguably the best studied stratigraphic units in western China. A series of lengthy reports has been published on this subject, which are the results of more than 10 years of systematic studies in the region. These reports discuss regional biostratigraphic correlation of these marine units [Tang *et al.*, 1992]. They also provide general background for paleoecology and depositional environments of Late Cretaceous-early Tertiary fossils including gastropods [Pan, 1990], enchinoids [Yang, 1991], brachiopods [Sun, 1991], nanofossils [Zhong, 1992], and ostracod fauna [Yang *et al.*, 1995] in the northern and western Tarim basin.

Tertiary biostratigraphy of the Kuche basin has also been extensively investigated based on studies of foraminifera, bivalves, algae, ostracoda, pollens, and gastropods [Xinjiang BGM, 1981; Hao *et al.*, 1982; Zhang *et al.*, 1986; Lu and Luo, 1990; Ye and Huang, 1990]. The nomenclature of the Tertiary stratigraphic units used in this study follows that of Ye and Huang [1990], who divided the Tertiary strata into the upper and lower sequences based on both their lithology and fossil content (Figure 8a).

4.1.1. Lower sequence. About 200-600 m thick and deposited mostly in a marine setting, the lower sequence consists of the Kumukeliemu group, which has been further divided into the Talake, Xiaokuzibai, and Avate Formations (from older to younger) (Figure 8a). The Kumukeliemu group is named after the Kumukeliemu anticline north of Baicheng, where the section was first established [Ye and Huang, 1990] (see Plate 1 for location). In the lower part of the Kumukeliemu group, the Talake Formation (150-200 m thick) consists of conglomerate beds in its lower part, fine-grained sandstone interbedded with thin dolomite layers in the middle part, and gypsum-bearing mudstone interbedded with siltstone in the upper part [Zhang *et al.*, 1986]. This unit deposited in a marine setting and is considered to be late Paleocene to early Eocene

in age based on its fossil content. It contains ostracoda (*Neocyprideis galba* (Mandelstam), *Loxococoncha* aff. *laculata* Mandelstam, and *Cytheretta* (?) cf. *insinuata* Mandelstam), bivalves (*Modiolus* sp., *Tellina* sp., and *Sphenia* sp.), and gastropods (*Ampullina* sp., *Natica* sp., *Turittella* sp., and *Polamides* sp.).

The Xiaokuzibai Formation (~230 m thick) directly above the Talake Formation consists of red gypsum-bearing mudstone interbedded with siltstone [Zhang *et al.*, 1986] (Figure 9a). It was also deposited in a marine setting and contains bivalves (*Polamides* sp.), ostracoda (*Neocyprideis galba* (Mandelstam)), and foraminifera (*Nonion* sp.). These fossils are assigned to the middle Eocene [Zhang *et al.*, 1986; Ye and Huang, 1990]. The Avate Formation (< 250 m) above the Xiaokuzibai Formation in the upper Kumukeliemu group consists of interbedded purple and gray mudstone. No fossils have been found in this unit.

Terrestrial beds are locally interbedded with the Kumukeliemu group in which algae (*Gyrogona qianjiangica* Z. Wang, and *Sphaerochara rugulosa* Z. Wang, *Gobichara* cf. *deserta* Karozewska et Ziembinska-Tworzydks) have been found [Lu and Luo, 1990]. According to Ye and Huang [1990], these algae are widely distributed in the middle Eocene to early Miocene strata throughout China. In summary, the Kumukeliemu group in the Baicheng area is best dated biostratigraphically as between the late Paleocene and early Miocene.

4.1.2. Upper sequence. About 1.2-1.6-km thick, the upper sequence consists entirely of terrestrial deposits and is divided, from older to younger, into the Suweiyi, Jidike, Kangcun, Kuche, Xiyu, and Wusu Formations. Biostratigraphy of the sequence has been well studied near the village of Jidike, northeast of Kuche (see Plate 1 for location). According to Ye and Huang [1990], the Suweiyi Formation (~200-400-m thick) is conformably on top of the Kumukeliemu Group, some 120 km to the west along strike (Plate 1). Here the Kumukeliemu Group was established mostly by lithologic correlation to its standard biostratigraphic section. The Suweiyi Formation is a sequence of interbedded gypsum-bearing mudstone and fine-grained sandstone. It contains ostracoda (*Eucypris longa* Mandelstam, *Cyclocypris cavernosa* Mandelstam, *Cyprideis littoralis* (Brady) *Dawinula stevensuni* (Brady et Robertson)) and algae (*Dongmingochara zhangjuheensis* (Xinlun), *Sphaerochara rugulosa* (Z. Wang), *Maedlerisphaera chinensis* (Huang et Xu Chara) *lepta* (S. Wang), *Granulichara longovalis* (S. Wang), *G. ovalis* (Mandler), *Gyrogona qianjiangica* (Z. Wang), *tephanochara* sp., *Hornichara* sp. nov., and *Croftiella zhui* (S. Wang)), whose ages range from Eocene to Early Miocene [Ye and Huang, 1990].

Above the Suweiyi Formation is the Jidike Formation (600-800 m thick) (Figure 8a), which consists of interbedded medium-grained sandstone and mudstone [Ye and Huang, 1990]. This formation contains abundant fossils, which include ostracoda (*Cyprinotus* (*Heterocypris*) *orientalis* Mandelstam, *C. (H.) incurvus* Galeeva, *C. (H.) formalis* Mandelstam, *C. (H.) ampullus* Mandelstam, *C. (H.) detaria* Galeeva, *Eucypris longa* Mandelstam, *E. concinna* Schneider, *Cyprina acutus* Galeeva, *Pseudoeucypris kerkiensis* Gramm, *Hemicyprinotus valvaetumidus* Mandelstam, *Mediocypris schneiderae* Galeeva, *Cypridopsis arctica* Jiang, *Limnocythere picturata* Suzin, *Darwinula silentiosa* Jiang, *Cypris* sp.1, *Eucypris* sp. 1, *Candona* sp. 1, *Cyprinotus* (*Heterocypris*) cf. *vialovi* Schneider, and *Cyprideis stephensoni* Sandberg) and algae (*Dongmingochara zhangjuheensis* (Xinlun), *Hornichara* sp. nov., *Sphaerochara rugulosa* Z. Wang, *Maedlerisphaera chinensis* Huang et Xu, Chara *lepta* S. Wang, *Granulichara ovalis* (Mandler), *G. longovalis* (S. Wang), *Nitellopsis* (*Tectochara*) *meriani* (Al Braun et Unger),

Strata Division	Approximate Age Based on Fossils	Formation Names
Upper Sequence	unknown	Wusu Formation
	unknown	Xiyu Formation
	Pliocene	Kuche Formation
	Miocene	Kangcu Formation
	Oligocene-Miocene	Jidike Formation
	Eocene-early Miocene	Suweiyi Formation
Lower Sequence (Kumukeliemu Group)	unknown	Avate Formation
	middle Eocene	Xiaokuzibai Formation
	late Paleocene-early Eocene	Talake Formation

Figure 8a. Nomenclature of Cenozoic stratigraphic units in the Kuche region. Basis for age assignment is discussed in text.

N. (T.) globula (Madler), *N. (T.) huangi* (Lu), *Rhabdochara stockmans* L. Grambast, *Croftiella zhui* (S. Wang), and *Lychrothamnus duplicicarinata* (Papp) [Xinjiang BGM, 1981; Ye and Huang, 1990; Lu and Luo, 1990]. The ages of the algae range from the Oligocene to the Miocene [Lu and Luo, 1990], and the ostracoda are considered to be Miocene in age [Ye and Huang, 1990].

The Kangcun Formation (300- 800 m thick) (Figure 8a) consists of interbedded mudstone, siltstone, and locally pebble conglomerate in its lower part and siltstone and sandstone in its upper part. Fossils found in this formation include ostracoda (*Eucypris concinna* Schneider, *Pseudocypris chinensis* Jiang, *Hemicyprinus valvaetumidus* Mandelstam, *Cyprinotus (Heterocypris) orientalis* Mandelstam, *C. (H.) phiaselus* Galeeva, *Candona Leei* Mandelstam, *Candona (Pseudocandona) subaequalis* (Jones), *C. (Lineocypris) asseptis* Galeeva, *Paracandona euplectella* (Brady et Norman), *Cypris acutus* Galeeva, *Mediocypris schneiderae* Galeeva, *Cycloocypris cavernosa* Mandelstam, *Ilyocypris manasensis* Mandelstam, *Zonocypris membranace* Livaltal, and *Cyprideis littoralis* (Brady)) and algae (*Dongmingochara zhangjuheensis* (Xinlun), *Hornichara* sp. nov., *Sphaerochara rugulosa* Z. Wang, *Maedelerisphaera chinensis* Huang et Xu, *Chara lepta* S. Wang, *Grambastichara zhui* (S. Wang), *Granulichara ovalis* (Madler), *G. longovalis* (S. Wang), *Nitellopsis (Tectochara) meriani* (Al. Brau et Unger), *N. (T.) globula* (Madler), *N. (T.) huangi* (Lu), *N. (T.) supraplana* (Peck et Reker), and *Croftiella shui* (S. Wang))

[Xinjiang BGM, 1981; Lu and Luo, 1990; Ye and Huang, 1990]. Although some of the fossils are the same as those found in the Suweiyi and Jidike Formations below, most are distinctive from those below. The age of the individual species ranges from Oligocene to Miocene [Ye and Huang, 1990].

Lithologically, the Kuche Formation (300-700 m thick) is dominated by coarse-grained sandstone and conglomerate (Figure 8a). In addition, minor thinly bedded mudstone and siltstone are also present [Ye and Huang, 1990]. Biostratigraphically, it contains ostracoda (*Subulacypris acris* Jiang, *Candona (Typhlocypris) Lonus* Jiang, *Cycloocypris regularis* Schneider, *Candona (Lineocypris) namanganica* Schneider, *C. (L.) seepis* Galeeva, *Candonan compressa* (Koch), *Candoniella albicans* (Brady), *Cypris decaryi* Gauthier, *Ilyocypris bradyi* Sars, *Cyprideis littoralis* (Brady), and *C. stephensoni* Sandberg subsp. no) [Xinjiang BGM, 1981; Ye and Huang, 1990], among which *Cycloocypris regularis* and *Candona (Lineocypris) namanganica* are Pliocene in age [Ye and Huang, 1990]. The younger Xiyu (50-1600 m thick) and Wusu (40-300 m thick) Formations are a sequence of conglomerates with unknown ages of deposition.

4.2. Lithostratigraphy

Tertiary lithostratigraphy was investigated in detail in two sections in this study (Figures 8b and 8c). The first is across the southern limb of a syncline along a big bend of the Kuche

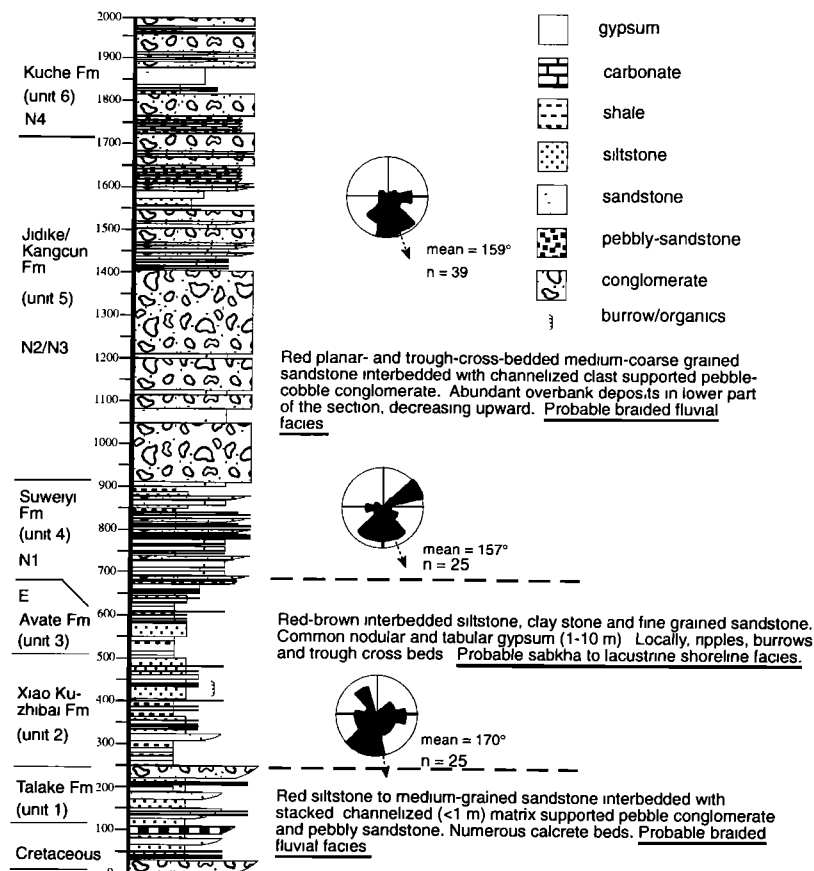


Figure 8b. Simplified stratigraphic section along the Kuche river, see Plate 1 for location. Scale is in meters. N1 to N4 are map units shown in Figure 5. Units 1 to 6 are lithostratigraphic units defined in this study (see Craig [1995] for detailed description). Their possible correlation with the biostratigraphic units of Ye and Huang [1990] is also indicated.

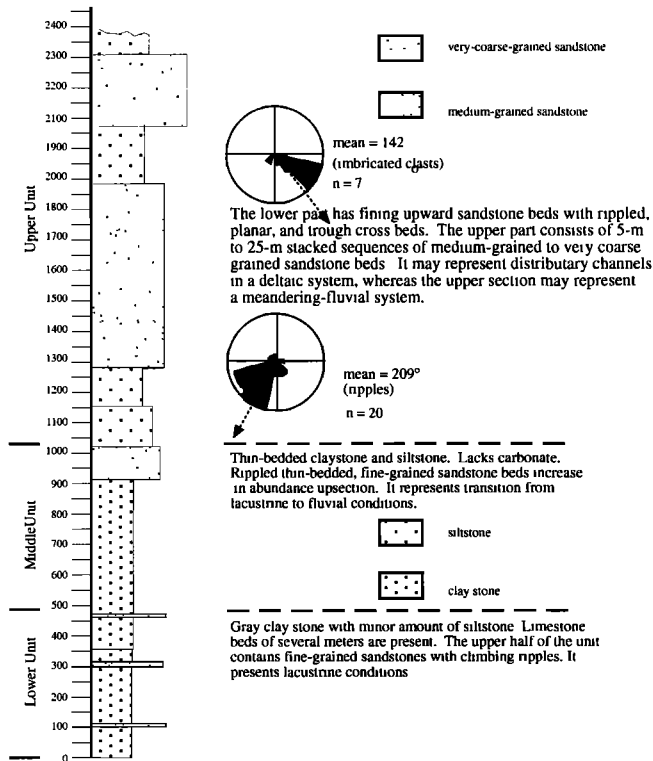


Figure 8c. Simplified stratigraphic section of the Bestantuogela area. See Plate 1 for location.

River directly north of Kuche city, and the second is along the Bestantuogela River northeast of Kuche (Plate 1). The two sections are located between the biostratigraphically controlled Kumukeliemu and Jidike sections. The detailed lithologic description and the basis for interpreting depositional environments of each stratigraphic unit discussed below are given by Craig [1995]. In the following, we summarize the main features of our measured sections and correlate them with the biostratigraphic units of Ye and Huang [1990].

4.2.1. Kuche section. Following Xinjiang BGM [1966c], the Upper Cretaceous strata consist of two members in the area (Figure 8b). The lower one is composed of a brown-gray conglomerate with a variable thickness but generally less than 20 m. The conglomerate is clast supported with a sandy matrix and shows scouring at its base. The clasts consist of marble, quartzite, chert, and indurated sandstone, possibly derived from the Paleozoic strata in the interior of the Tian Shan. The upper member is an upward fining sequence from pebble conglomerate and coarse sandstone to interbedded mudstone and sandstone, probably resulting from transgression of a shallow sea as discussed by Sobel [1995].

Six lithological units are divided in the measured Tertiary section. Unit 1 in the basal part lies conformably on top of the Cretaceous strata. From older to younger, it consists of three members: (1) a 28-m-thick sandstone and conglomerate unit which forms a prominent ridge and is laterally persistent throughout most of the Kuche basin [Ye and Huang, 1990], (2) poorly sorted sandstone and clay stone with lenses of cross-bedded, coarse sandstone overlain by gypsum-rich clay stone (~42 m thick), and (3) 55-m-thick poorly sorted mudstone with pebbles and gypsum nodules. We interpret the unit to have been deposited in a braid delta (see Craig [1995] for detailed discussion). The shifting of paleoshorelines caused facies

variation within the measured section. The gypsum nodules may represent saline-mudflat facies of a marginal-marine sabhka [Sobel, 1995]. Lithologically, this unit correlates to the Talake Formation of Ye and Huang [1990].

Unit 2 (215-m thick) is conformably on top of unit 1. It consists primarily of clay stone and siltstone, with thin to thick beds of fine-grained sandstone. There are several intervals of upward fining and coarsening sequences in this unit. Some can be clearly identified as Bouma sequences. Gypsum is present as both concentrated nodules and beds of solid gypsum. This unit may have deposited during a transgression from coastal mudflats of a river-dominated shoreline to marine turbidites [e.g., Blatt et al., 1980; also see Craig, 1995; Sobel, 1995]. Its lithology correlates with the Xiaokuzibai Formation of Ye and Huang [1990].

Unit 3 (180-m thick) has a gradational contact with unit 2. Its lower part is dark-red claystone with thin beds of gypsum and thin-rippled sandstone beds, above which is massive siltstone and interbedded clay stone and fine-grained sandstone. The formation has an overall upward coarsening trend represented by the increasing abundance of sandstone beds. The unit may represent the saline-mudflat facies of a marginal marine sabhka, marking the last phase of marine deposition [e.g., Blatt et al., 1980; also see Craig, 1995; Sobel, 1995]. As the Avate Formation of Ye and Huang [1990] is composed of interbedded clay stone and fine-grained sandstones with the presence of gypsum beds, unit 3 is best correlated with this formation.

The contact between unit 4 and unit 3 is abrupt where channeling incision is present. This unit (246-m thick) consists of stacked 1 to 4-m-thick, fining-up sequences, which change from conglomerate, pebbly sandstone, and sandstone beds to poorly sorted clay stone and siltstone. The coarse beds pinch out over tens of meters, and smaller lenses show distinct channel geometries and basal scouring. Unit 4 may represent a change from a marine to braided-fluvial depositional setting [e.g., Blatt et al., 1980] and correlate with the Suweiyi Formation and possibly the lower part of the Jidike Formation of Ye and Huang [1990].

Unit 5 (1.6 km thick) is conformably on top of unit 4 and consists of stacked fining-up sequences from pebble conglomerate and pebble sandstone to medium-grained sandstone. Clay stone and siltstone beds (<5%) are present in the top half of the section. The conglomerate beds consist mainly of matrix-supported trough and planar cross beds. Overall, this unit represents a thick braided-fluvial sequence [e.g., Blatt et al., 1980]. We favor this interpretation over alluvial-fan deposition because of the lack of gravity-flow deposits. This unit probably correlates with the Jidike Formation and part of or the entire Kangcun Formation.

Unit 6 consists of a sequence of conglomerate (at least 300 m thick and possibly up to 2-3 km thick) locally interbedded with lenticular sandstone beds. The lithology of this unit correlates with the Kuche Formation of Ye and Huang [1990]. The presence of large boulders (>50 cm in diameter) in the sequence suggests that the unit may represent alluvial fan deposits.

Although the lack of fossils in our measured section makes its age assignment uncertain, the presence of gypsum beds in units 1-3 implies that they are lithologically correlated to the Kumukeliemu group and Suweiyi Formation in the standard section of Ye and Huang [1990]. This makes the marine-fluvial transition in unit 4 and the 1.6-km-thick braided-fluvial sequence in unit 5 younger than the early Oligocene.

Both point counts of the sandstone and clast counts of the conglomerates show an abrupt increase in metavolcanic components at the base of unit 4 and continuing into the overlying

strata [Craig, 1995]. Clasts of reworked sandstone are also found in the conglomerates. These changes may represent a change in the source area caused by thrusting-induced uplift in the southern Tian Shan, where late Paleozoic metavolcanic rocks are abundant [Carroll *et al.*, 1995]. The braided-fluvial sequence and the younger alluvial sequence (N1 to N-Q in Figure 5) are synfolding, as indicated by the shallowing in dip angles from overturned to about 40° in the forelimb of an anticline (Plate 1).

4.2.2. Bestantuogela section. This section begins in the Tertiary strata across the south limb of an anticline (Figure 8c). According to the geologic map of Kuche region [Xinjiang BGM, 1966c], the base of the section lies in the upper Miocene. Because no gypsum beds are present in the measured section as described below, the age of this section is most likely younger than the age of the early Oligocene-Miocene Suweiyi Formation of Ye and Huang [1990]. However, its exact age is unconstrained. We divide the Bestantuogela section into three units (Figure 8c). The lower unit (~490-m thick) is predominately gray-brown and blue-gray clay stone, with a minor amount of siltstone. Limestone is present as laminae or beds up to several meters thick. The upper half of the unit contains fine-grained sandstone beds, some with climbing ripples. We interpret this unit to have deposited in lacustrine conditions [e.g., Blatt *et al.*, 1980].

The middle unit (432 m thick) is predominately thin-bedded clay stone and siltstone. It lacks carbonate and has a higher proportion of silt than that in the lower unit. Although volumetrically small (<15%), rippled and thin-bedded fine-grained sandstone beds increase in abundance upsection. This unit may represent the transition from lacustrine to fluvial conditions [e.g., Blatt *et al.*, 1980].

The upper unit (1358 m thick) has an abrupt contact with its underlying unit. Its lower part has fining upward sandstone beds, which are rippled and planar- and trough-cross-bedded. The upper part is composed of 5-m- to 25-m-thick stacked sequences of medium-grained to very coarse grained sandstone beds. They are commonly rippled and planar cross-bedded. The beds have distinctive channel geometries and epsilon cross beds. The sandstone beds are fining upward to become siltstone and claystone beds, which are commonly laminated. The entire unit is characterized by an increase in the abundance of sandstone beds upsection, indicating a relative increase in sediment supply or energy change. The lower part of this unit may represent distributary channels and interchannel areas in a deltaic system, whereas its upper part may represent a meandering-fluvial system (e.g., Blatt *et al.* [1980], also see Craig 1995 for detailed discussion).

4.3. Magnetostratigraphy

4.3.1. Sample preparation and laboratory measurements. In order to constrain ages of the Kuche basin, we conducted a magnetostratigraphic investigation of the Kuche and Bestantuogela sections. Oriented hand samples, typically 10 x 10 x 5 cm in size, were collected in the field. Preference was given to well-indurated mudstone and fine-grained sandstone. Samples were collected at ~50-m intervals in the Bestantuogela section and the fluvial part of the upper Kuche section. Samples were collected at ~20-m intervals in the lower part of the Kuche section, consisting of lacustrine-sabkha deposits. This sample spacing is somewhat larger than others reported [e.g., Burbank and Johnson, 1983; Burbank *et al.*, 1992; Harrison *et al.*, 1993], because of the reconnaissance nature of the project and access to appropriate lithology. A total of 81 sites were collected from the two sections. Sam-

ples from 6 of the 81 sites were destroyed during shipping. The surviving samples were drilled into 1.5-cm-diameter cores. Ideally, at least three cores were obtained from each sample, but in practice, samples from 47 sites yielded three or more cores, and 28 produced one or two specimens.

The characteristic remnant magnetism (ChRM) of each sample was measured using a cryogenic magnetometer in the laboratory of Joseph Kirschvink at the California Institute of Technology. The procedure of our sample analysis follows that of Butler [1992]. The natural remnant magnetism (NRM) of each specimen was measured first. Next, specimens from selected sites were demagnetized using stepwise alternating-field (AF) demagnetization from 0 G to 800 G in 50-G intervals. Sites whose characteristic component of NRM (ChRM) was not clearly resolved by AF demagnetization were then subjected to thermal demagnetization; samples were heated stepwise to 680°C by 100°C-increments from 150° to 450°C and in 25°C-increments from 500°C to 650°C.

In general, the results from the two sections varied significantly in their quality and reliability. This is, in large part, due to the grain sizes available for sampling. The Bestantuogela samples consist primarily of siltstone and very fine-grained sandstone, whereas the Kuche samples are typically siltstone to fine-grained sandstone in the lower part and medium-grained sandstone in the upper braided-fluvial sequence.

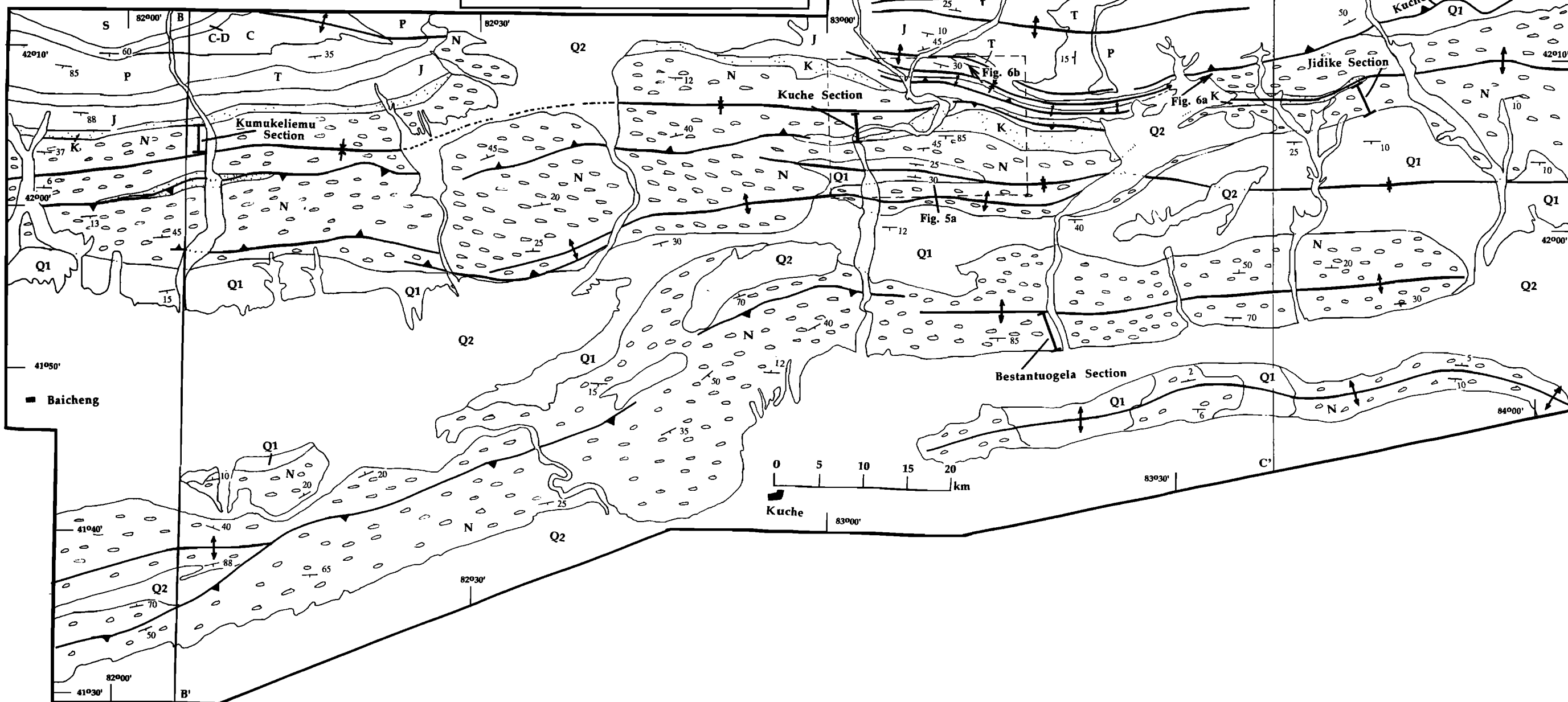
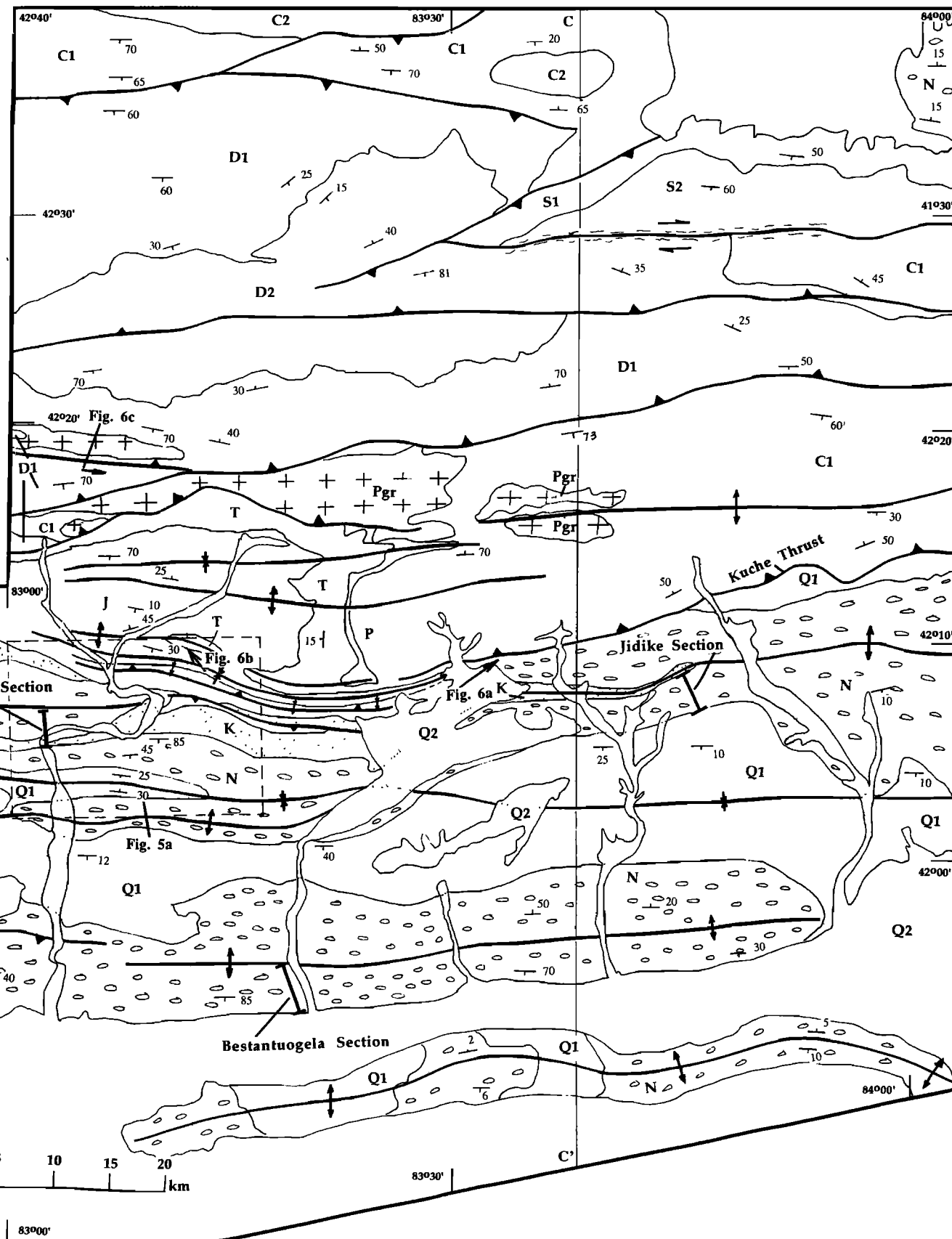
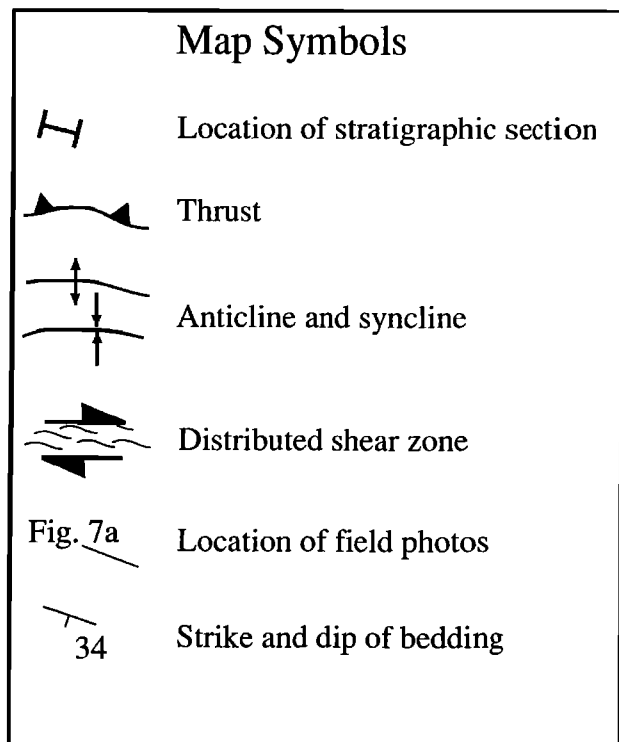
When the ChRM revealed by demagnetization is compared to the original NRM, we found that the majority of samples received very little postdepositional overprinting. After demagnetization, the samples from the two sections passed both the reversal and fold tests [e.g., McElhinny, 1973].

The mineralogy of the samples was revealed in the *J/J₀* plot [Craig, 1995], which is a magnetic intensity plot showing the loss of intensity after each step of demagnetization. *J* represents the magnitude of the magnetic vector and *J₀* represents the original intensity. The plot shows that the dominant mineral in the Bestantuogela section is titanomagnetite, as indicated by the large reduction in NRM during AF demagnetization [Butler, 1992]. The magnetism present after the sample was heated to the Curie temperature of the titanomagnetite (575°C) is due to the presence of titanohematite, which has a Neel temperature of 670°C and sometimes retains magnetism up to 725°C. The samples from the Kuche section typically retained their levels of magnetic intensity to higher temperatures and are less sensitive to AF demagnetization. NRM in those samples is due to a larger component of titanohematite.

The final results were analyzed using spherical statistics. The quality of all the sites was classified into three groups, using the Fisher *k* statistic for dispersion on a sphere [Fisher, 1953]. If the magnetic directions from at least three samples from a site were in close agreement (*k* > 10), then the site was classified as class I. If two samples were in close agreement, while the third was not (*k* < 10) or if less than three samples were analyzed from a site, then the site is classified as class II. If there was little agreement between the samples or if only one sample for a site was recovered, then it is a class III site. Class III sites were not used in the magnetic-polarity sections, unless only one sample was recovered and that sample had a clear ChRM direction. With this classification in data quality, the Kuche section consists of 34%, 23%, and 43% of class I, II, and III sites, respectively. In contrast, the Bestantuogela section is composed of 61%, 27%, and 12% of class I, II, and III sites, respectively.

4.3.2. Correlation to the magnetic-polarity timescale. A determination of the time interval represented by the section would improve the correlation with the magnetic-polarity timescale. Estimates for the time represented by

Plate 1. Geologic map of the Kuche area based on both the geologic map of the Kule region [Xinjiang BGM, 1966c] at a scale of 1:200,000 and our own mapping at a scale of 1:50,000 along the Kuche River. Abbreviations are as follows: Q1, and Q2, Quaternary alluvial deposits; N, Neogene lacustrine and fluvial deposits; K, Cretaceous strata, locally includes the Paleogene strata; J1, lower section of Jurassic strata; J2, upper section of Jurassic strata; P, Permian strata; T, Triassic strata; C, Carboniferous strata; D, Devonian strata; and Pgr, Permian granitoids. Location of cross sections BB' and CC' shown in Figure 4 and location of Figures 5a, 6a, 6b, and 6c are indicated.



the stratigraphic column are important in this case because of the lack of a precise age horizon within the column. Although with some uncertainties, sedimentation rates on timescales of >1000 years are typically of the order of 0.1 m ka⁻¹ in a wide range of depositional systems and tectonic settings [Sadler, 1981]. Typical rates of foreland-basin sedimentation are between 0.1 and 0.4 m ka⁻¹ [Johnson *et al.*, 1988; Burbank *et al.*, 1992; Harrison *et al.*, 1993], but rates as high as 0.9 m ka⁻¹ were also reported [Jordan *et al.*, 1988]. With this range of sedimentation rates, the stratigraphic columns can be scaled to various ranges and compared with the magnetic-polarity time scale.

Another method is to estimate the time represented by the magnetostratigraphic column using a numerical model, which relates the average time between magnetic reversals, style of sampling (e.g., uniform, random, etc.), sample spacing, and number of reversals within the section. We applied the model developed by Johnson and McGee [1983], which has the following form, $Pu = \frac{1}{2} [1 - \exp(-2\Delta t/\tau N)]$, where Pu is the probability that a magnetic reversal lies between two samples, N is the sample spacing, Δt is the time represented by a stratigraphic section, and τ represents the average time between reversals. This model assumes that reversals follow an exponential probability distribution [Cox, 1981]. The total number of reversals Ru within a stratigraphic section is $Ru = Pu(1-N)$. From these relations, the amount of time represented by a stratigraphic column can be calculated. We applied this model to estimate the time duration of both the Kuche and Bestantuogela sections as a whole and in part. The calculated results indicate that the fluvial sequence of the Bestantuogela section, which is 1130 m thick, had been deposited over 4.5 m.y. (see Craig [1995] for details). This yields a sedimentation rate of 0.25 m ka⁻¹, consistent with the range of sedimentation rates in a foreland basin estimated by others as mentioned previously.

The key assumption in our correlation is that the youngest age of the gypsum-bearing strata in the Kuche foreland basin correlates with the early Oligocene-Miocene Suweiyi Formation. This makes the sequence above the gypsum beds in the Kuche section late Oligocene or younger in age. Because no gypsum beds are present in the Bestantuogela section, it should also be late Oligocene or younger in age according to our lithological correlation to the biostratigraphy of Ye and Huang [1990].

The measured magnetostratigraphic section was correlated using the best interpretive fit to the magnetic-polarity timescale of Cande and Kent [1992] (Figure 9). Because of fewer high-quality sample sites in the Kuche section, its correlation to the magnetic timescale is problematic. In contrast, the Bestantuogela section provides an excellent fit (Figure 9). This fit resulted from numerous tests of changes in assumptions: (1) we allowed sedimentation rates to vary by a factor of 2; (2) we examined changes in rates in the top and bottom of the Bestantuogela section; and (3) we compared the column with all of the Oligocene through Pliocene reversals. The best correlation of the Bestantuogela section with the magnetic-polarity timescale requires the sedimentation rate to be 0.2 m ka⁻¹. Note that the poor correlation in the basal part of the Bestantuogela section is the result of both the large number of small reversal events which occurred during this time interval and wide sample spacing which may have caused several events to be unrecognized.

The good fit of the Bestantuogela section may be, in turn, used to constrain the age of the magnetically poorly defined Kuche section if the facies relationship between the two sections can be established. One possibility is that the lacustrine-to-fluvial transition in the Kuche section matches the deltaic-to-meandering fluvial transition in the Bestantuogela section (Figure 9a). This correlation also matches the magnetic-polarity distribution in both sections and implies that the lacustrine-to-fluvial transition occurred at ~21 Ma. Another possible correlation is between the lacustrine-to-fluvial transition in the Kuche section with the lacustrine-to-deltaic transition in the Bestantuogela section. This would place the transition in the Kuche section at ~24 Ma.

trine-to-fluvial transition in the Kuche section matches the deltaic-to-meandering fluvial transition in the Bestantuogela section (Figure 9a). This correlation also matches the magnetic-polarity distribution in both sections and implies that the lacustrine-to-fluvial transition occurred at ~21 Ma. Another possible correlation is between the lacustrine-to-fluvial transition in the Kuche section with the lacustrine-to-deltaic transition in the Bestantuogela section. This would place the transition in the Kuche section at ~24 Ma.

4.4. Timing of Thrust Initiation in the Southern Tian Shan

The timing of Cenozoic thrust initiation in the Tian Shan has been variably estimated to be between Oligocene and Pliocene. On the basis of rapid increase in sedimentation rates indicated by biostratigraphy established by the Chinese workers [e.g., Ye and Huang, 1990], Windley *et al.* [1990], Allen *et al.* [1991, 1993], and Yin and Nie [1996] inferred that thrusting in the Tian Shan initiated between Oligocene and Early Miocene. Although the exact age assignment of the last marine deposits in Tarim may be either late Oligocene or early Miocene [Ye and Huang, 1990] and a large global eustatic regression of 100-200 m occurred during the Oligocene [Haq *et al.*, 1987], the present elevation of these marine deposits at 1-2 km in the southern Chinese Tian Shan suggests that its uplift must have occurred after the late Oligocene. If we attribute the uplift to crustal thickening due to thrusting in the southern Tian Shan thrust belt, then thrusting should have initiated after the late Oligocene.

Apatite fission track analysis of Mesozoic strata on the northern flank of the Chinese Tian Shan yields a consistent 24±4 Ma cooling age, which indicates the time of denudation in the Tian Shan, possibly related to tectonically induced rapid uplift of the range at the time [Hendrix *et al.*, 1994]. Taking the same approach, Sobel and Dumitru [1997] sampled Miocene strata in the western part of the southern Chinese Tian Shan thrust belt (i.e., their Kuzigougsu and Wenguri sections). Their data indicate that unroofing in sediment source areas cooled rocks through about ~100°C beginning in the Oligo-Miocene (23-25 Ma) and continued through the mid-Miocene (~13-16 Ma). They inferred the source area in the south central Chinese Tian Shan (i.e., north of the Baicheng-Kuche thrust belt).

The above estimated timing for the initiation of thrusting in the Tian Shan, that is, between late Oligocene and early Miocene is consistent with the inference derived from the Quaternary shortening rate and the total amount of Cenozoic shortening across the Tian Shan [Avouac *et al.*, 1993]. In contrast to this estimate, a high rate of N-S shortening ~20±3 mm yr⁻¹ has been recorded by a Global Positioning System survey in the westernmost part of the Tian Shan in Kirgikstan [Abdrakhmatov *et al.*, 1996]. This rate together with the estimated 200-km Cenozoic shortening in the western Tian Shan places the thrust initiation at about 10 Ma.

Initiation of Cenozoic thrusting in the Kuche basin may be indicated by the transition from the lacustrine to fluvial facies in both the Kuche and Bestantuogela sections at about 24-21 Ma. The dramatic facies changes in the two sections at this location may reflect the effect of thrust loading in the southern Tian Shan. However, as pointed out by Jordan *et al.* [1988], an increase in the input of sediments to a foreland basin may or may not be related to thrusting, depending on whether climate conditions were changed, which may increase or decrease the power of erosion. However, a marked increase in metavolcanic fragments in units 4 and 5 of the Kuche section beginning in

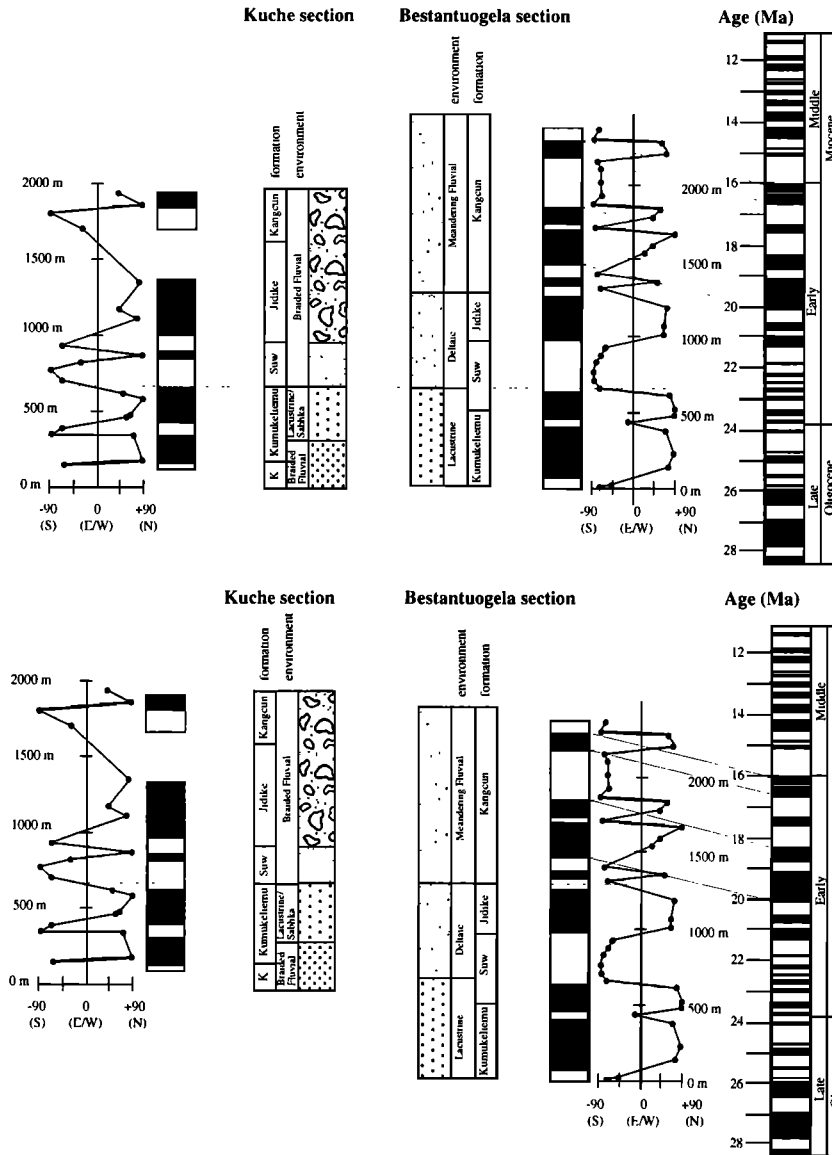


Figure 9. Magnetic-polarity stratigraphy of the Kuche River and Bestantuogela sections. Two possible facies correlations between the Bestantuogela and Kuche sections are shown. (a) The lacustrine-braided fluvial transition in the Kuche section correlates to the lacustrine-deltaic transition in the Bestantuogela section. This correlation implies time transgression for the same facies in different locations of the basin. (b) The lacustrine-braided transition in the Kuche section correlates with deltaic-meandering fluvial transition. The first correlation implies that the initial input of coarse clastic sediments in the Kuche basin began at about 24 Ma, where the second implies an age of 21 Ma. Magnetic-polarity timescale is based on *Cande and Kent* [1992].

this time interval implies exposure of new and deeper source areas brought up by south verging thrusting. This is a common thrust-related process in foreland basins [e.g., *Jordan et al.*, 1988]. If our estimate of timing for the thrust initiation (21-24 Ma) is correct, using the estimated magnitude of shortening (20-40 km) and shortening strain (20-30%), the slip and strain rates in the southern Chinese Tian Shan thrust belt yield 1-1.9 mm yr⁻¹ and 2.9-4.5x10⁻¹⁶ s⁻¹, respectively.

Two factors may complicate the above interpretation. First, as the development of thrusts may propagate outward from the core of the Tian Shan to the north and south, the timing of the observed facies changes may only indicate the initiation of a younger and more southern thrust system. The sedimentological record in response to an older and more northern thrust sys-

tem may have been eroded away in the hanging wall of the southern thrust system. This kinematic history implies that 24-21 Ma is the minimum age of thrust initiation in the southern Chinese Tian Shan. However, we argue that the initiation of thrusting cannot be older than the Oligocene (~36-24 Ma), the time of last marine deposition in the northern Tarim basin and southern Tian Shan [e.g., *Ye and Huang*, 1990]. As these marine strata are not at elevations between 1.5 and 2 km, they must have been uplifted by tectonism but cannot be caused solely by sealevel change, which is only of the order of some 100-200 m during this time interval [*Haq et al.*, 1987].

Another complexity involving dating initiation of thrusting is that deposition of conglomerates in the distal area may be related to cessation of thrusting, whereas deposition of fine-

grained sediments was related to the process of thrust loading and thus dates the timing of thrust movement [e.g., Heller *et al.*, 1988]. If this is the case for the Kuche and Bestantuogela sections, then the age of thrusting should have begun even earlier than the estimated 24-21 Ma. However, the relationship between folds and the synfolding braided-fluvial sequence in the Kuche section rejects the second proposal but permits the first possibility. As evident in Figure 5, this Neogene sequence (N1 to N-Q1 in Figure 5) was deposited during folding, as indicated by the systematic decrease in dip angle as the strata become younger (Figure 5). The oldest age of the growth strata, which is approximately located at the base of the braided-fluvial sequence, places constraints on the initiation age of folding and thrusting [e.g., Suppe *et al.*, 1992].

5. Structural Evolution of the Baicheng-Kuche Thrust System

On the basis of the structural relationship and sedimentological studies in the Kuche area, a kinematic model is proposed that explains the timing of thrusting and its relationship to sedimentation in the Kuche basin (Figure 5). The first Cenozoic contractional structure began to develop at 24-21 Ma in

the northern part of the Baicheng-Kuche thrust system (Figure 10a). We tentatively assigned the strike-slip shear zone and adjacent thrusts in Plate 1 as Paleozoic structures. We interpret the bedding-parallel fault in the middle Jurassic strata to have initiated at this time. It could be geometrically linked with the main thrust to the north. This event led to the exposure of the Paleozoic-Mesozoic stratigraphic section in the hanging wall of the thrust and deposition of the fluvial-alluvial sequence (Figure 5) in the footwall in the southern part of the thrust system. The alluvial-fan facies has been eroded away because of development of younger thrusts to the south, which exposes the braided fluvial sequence in the footwall of the older thrust (Figures 10b-10d). The Kuche thrust began to develop in the footwall of the older thrust (Figures 10b and 10c). Its initiation produced a fault-propagation anticline and shed coarse-grained sediments southward, recorded by the deposition of the alluvial fan sequence. The development of the older thrust, the Kuche thrust, and the younger minor thrusts and folds produced the synfolding sequence of sedimentation (Figures 10c-10e)

6. Denudation of the Chinese Tian Shan

In order to constrain the paleotopographic history of the Tian Shan, the denudation and crustal-shortening histories of

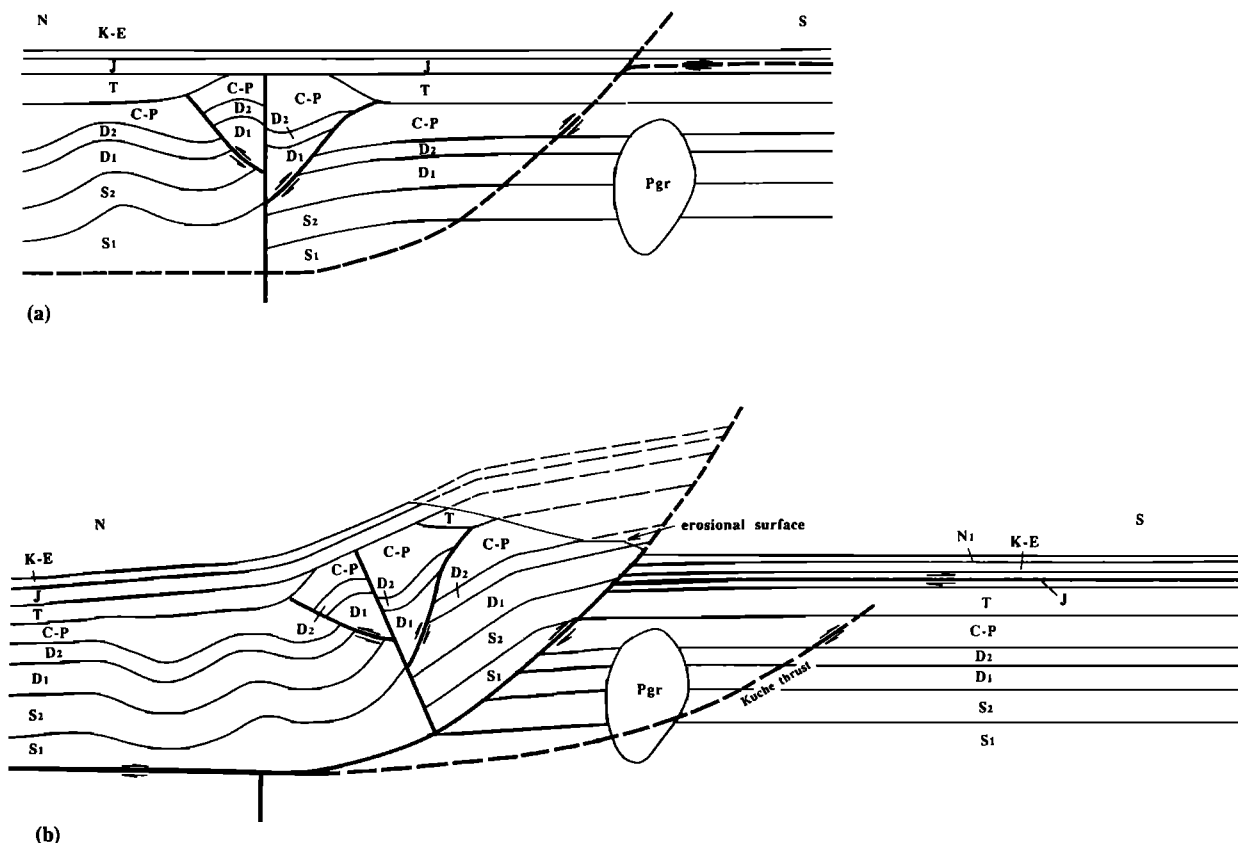


Figure 10. Structural evolution of the Baicheng-Kuche thrust system and its relationship to the stratigraphic development. (a) At 24-21 Ma, the initiation of an early thrust in the northern part of the thrust system and an associated bedding-parallel thrust lying within the Jurassic strata and deposition of lacustrine sediments (N1). (b)-(c) At 21-14 Ma, the Kuche thrust began to develop, which deformed an older bedding-parallel thrust in the Jurassic strata and shed sediments to the south, and deposition of fluvial sediments in the Kuche section (N2¹). (d)-(e) Further development of the Kuche thrust and its footwall thrusts and folds deformed the earlier deposits (N1 and N2¹) and syn-tectonic sediments (N2²-Q) have been deposited and tilted while thrusting was ongoing.

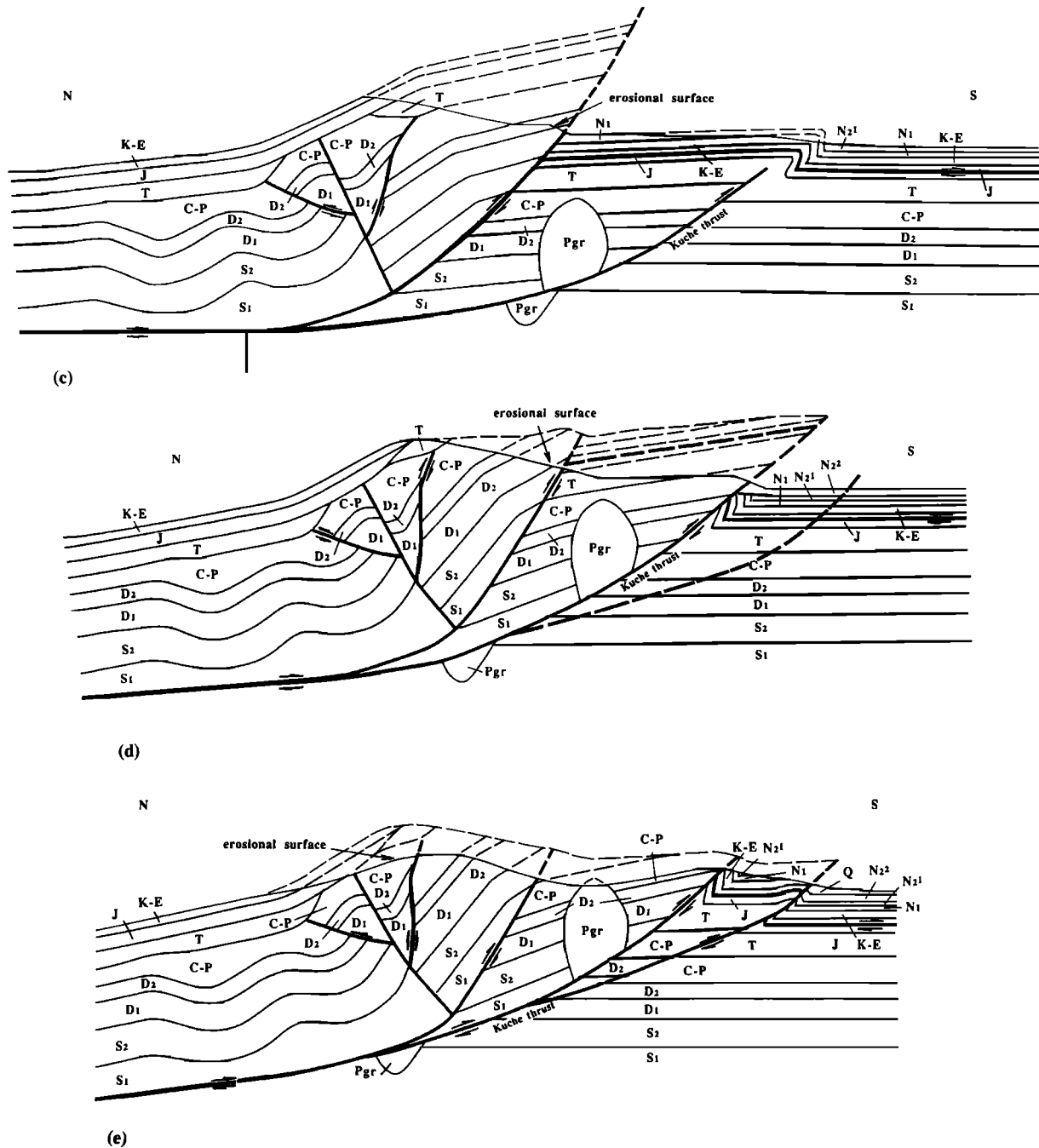


Figure 10. (continued)

the mountain range must be known. As no Cenozoic normal faulting has been identified in the Tian Shan region, its denudation may be entirely attributed to contractile uplift and erosion: the N-S contraction contributes to the increase in elevation of the Tian Shan, whereas erosion reduces it. We have previously discussed the constraints on the timing and magnitude of shortening in the southern Tian Shan. In this section, we present results of $^{40}\text{Ar}/^{39}\text{Ar}$ thermochronological analyses to constrain the magnitude and timing of erosion in the Tian Shan.

Igneous intrusive rocks with emplacement ages ranging from Precambrian to early Mesozoic time are widespread in the

Chinese Tian Shan [Xinjiang Regional Mapping Team, 1985] (Figure 1c), which provides an excellent opportunity for performing $^{40}\text{Ar}/^{39}\text{Ar}$ analysis. Two sampling traverses were conducted for $^{40}\text{Ar}/^{39}\text{Ar}$ analysis: one along the Urumqi-Korla highway in the eastern Chinese Tian Shan, and the other along the Kuche-Dushanzi highway in the central Chinese Tian Shan (Figure 1c). Most samples were collected from late Paleozoic granitoids, but a few were collected from a zone of mylonitic gneisses along the axis of the central Tian Shan (Figure 1c).

Mineral separates of K-feldspar, hornblende, and biotite were obtained from fresh hand specimens. For the $^{40}\text{Ar}/^{39}\text{Ar}$ analyses, mineral separates were irradiated together with Fish

Table 1. Summary of $^{40}\text{Ar}/^{39}\text{Ar}$ Ages

No.	Rock Type	Mineral	Location	Age Ma
N7*	granitoid	K-feldspar	Bayinbluke	297.3±1.1
				306.4±0.5
				308.3±0.6
N13*	mylonitic gneiss	muscovite	Central Tian Shan	301.8±1.1
				303.0±1.0
				313.7±2.6
N21*	granitoid	biotite	North Tian Shan	254.5±4.8 260.1±3.4
N23*	granitoid	K-feldspar	North Tian Shan	230.8±0.8
				240.4±1.4
				245.9±1.4
N39*	diorite rock	K-feldspar	South Tian Shan	224.2±0.8
				biotite
		hornblende		293.2±0.9 317.3±3.3
N70*	volcanic rocks	biotite	North Tian Shan	295.5±0.6
		K-feldspar		264.1±1.5 267.9±0.8
TS1†	mylonitic diorite	hornblende	East Tian Shan	262
		biotite		347
		K-feldspar		333
TS0†	mylonitic gneiss	biotite	East Tian Shan	286

* Laser fusion ages.

† Total gas ages calculated from step-heating results.

Canyon sanidine flux monitors for 45 hours in the H-5 position of the Ford Reactor, University of Michigan. Correction factors used for interfering neutron reactions were $(^{40}\text{Ar}/^{39}\text{Ar})_{\text{K}} = 0.0225$, $(^{38}\text{Ar}/^{39}\text{Ar})_{\text{Cl}} = 1.20 \times 10^{-2}$, $(^{37}\text{Ar}/^{39}\text{Ar})_{\text{Ca}} = 7.00 \times 10^{-4}$, and $(^{36}\text{Ar}/^{39}\text{Ar})_{\text{Ca}} = 2.90 \times 10^{-4}$. All the samples from the Urumqi-Korla highway were step heated in a Ta crucible within a double-vacuum furnace, and $^{40}\text{Ar}/^{39}\text{Ar}$ isotopic measurements were performed using a VG 1200S automated mass spectrometer operated in the electron multiplier mode. Details of flux monitor ages, neutron irradiation, step heating, and isotopic analyses are given by *Harrison et al.* [1992b]. Tabulated results of the argon isotopic analyses, uncorrected for neutron-produced interference except $(^{38}\text{Ar}/^{39}\text{Ar})_{\text{Cl}}$, are given in Table 1 using conventional decay constants and isotope abundances. Samples from the Kuche-Dushanzi highway were analyzed by the laser-heating technique.

The results of the $^{40}\text{Ar}/^{39}\text{Ar}$ analyses indicate that the dominant cooling ages of muscovite, biotite, hornblende, and K-feldspar for all the samples are in the range of 224-320 Ma, clearly indicating a thermal event which occurred in the late Paleozoic to early Mesozoic. As our structural investigation has focused only on the Cenozoic deformation, it is not clear whether the thermal event was related to denudation or magmatism. Nevertheless, from the closure temperatures of muscovite and biotite (~300°-350°C [*McDougall and Harrison, 1988*]) and reasonable assumptions regarding geothermal gradient (20°-30°C km⁻¹), the amount of post-Paleozoic erosion in the Tian Shan is no more than 12 km.

Fission track thermochronological analysis of samples from the north and south flanks of the Tian Shan by *Hendrix et al.*

[1994] suggests that only a 3 to 5-km-thick section of the crust has been eroded in the last 25 m.y. A more comprehensive apatite fission track analysis was recently conducted by *Zhou et al.* [1995] across the Tian Shan. Their traverse between Kuche and Dushanzi coincides with our western sampling route. They found that a Late Carboniferous granitoid along the northern margin of the central Tian Shan arc terrane cooled below 110°C at about 130 Ma. This Cretaceous cooling age may reflect tectonically induced denudation, which is recorded by the large flux of granitic clasts in the Cretaceous strata throughout the Chinese Tian Shan (*Hendrix et al.* [1992] and this study, see Figure 8a). Mylonitic granites in the central Chinese Tian Shan strike-slip shear zone (Figure 1) show apatite cooling ages between 24 and 10 Ma. $^{40}\text{Ar}/^{39}\text{Ar}$ thermochronological analysis of biotites, muscovites, and K-feldspars from mylonitic granites of the same shear zone shows no Cenozoic cooling [*Yin and Nie, 1996*]. The combined results of $^{40}\text{Ar}/^{39}\text{Ar}$ and apatite fission track analyses suggest that the amount of Cenozoic denudation of this mylonitic shear zone is no more than 10 km and that the overall Chinese Tian Shan has experienced little exhumation (<5 km) in the Cenozoic. This is in sharp contrast to that of the southern Tibetan plateau, where rapid and large denudation up to 20 km occurred between the late Oligocene and the middle Miocene [*Harrison et al., 1992a; Yin et al., 1994*].

7. Relationship Between Uplift, Denudation, and Crustal Shortening

The surface of the Earth is continuously altered under the influence of weathering, erosion, plate tectonics, deposition,

and volcanic processes. One of the goals of our investigation was to estimate both the elevation of the Tian Shan prior to late Cenozoic deformation and the elevation gained with respect to sea level since late Cenozoic deformation began. This may be achieved by interpreting the results of our geologic observations in the framework of a simple quantitative model based on the assumptions of conservation of mass, uniform crustal shortening, and Airy isostasy described below. As the uncertainty of our estimates on the magnitude and timing of both Cenozoic crustal shortening and exhumation in the Chinese Tian Shan is large (e.g., a factor of 2-4 in estimating the magnitude of shortening, depending on the assumption of thrust-fault geometry), the one-dimensional model presented below should be regarded as a conceptual guide rather than a realistic model at this stage. This model serves to demonstrate the need for well-distributed, high-resolution field data (i.e., crustal shortening and denudation) in reconstructing the paleoelevation history of the Tian Shan. Although not explored here, the biggest uncertainty in estimating the elevation history of a region is the effect of changes in thermal states in the lithosphere, which is difficult to quantify by surface geology.

The magnitude of uplift, U , of a mountain range at a point is the difference between its present elevation $e2(t)$ and its past elevation $e1(t_0)$ at a specific time t_0 with respect to the sea level (Figure 11),

$$U(t) = e2(t) - e1(t_0) \quad (1)$$

In general, the magnitude of this uplift is a function of time, as elevation of a mountain range changes because of horizontal shortening and denudation. By differentiating various mechanisms contributing to surface uplift, the total amount of uplift may be the summation of the following terms

$$U(t) = e2(t) - e1(t_0) = U_{loc} + U_{therm} - D \quad (2)$$

where U_{loc} is the surface uplift/elevation reduction due to lithospheric shortening/extension; U_{therm} is the surface uplift due to a change in the thermal gradient in the lithosphere and asthenosphere, which in turn causes changes in the density distribution and the surface elevation; and D is the amount of denudation due to either erosion or normal faulting.

It appears that the 2500-km-long Tian Shan is supported by different mechanisms in the mantle lithosphere along strike. According to seismological studies and analysis of averaged gravity data [Makeyeva et al., 1992; Kosarev et al., 1993; Roecker et al., 1993; Burov et al., 1990], the western Tian Shan between the Pamir and the Talas-Ferghana fault and the eastern Tian Shan in China have a cold lithospheric root. In contrast, the central Kirgыз Tian Shan is underlain by an anomalously low-velocity region in the upper mantle, implying a relatively elevated temperature. The low-velocity central Tian Shan coincides spatially with the presence of Cretaceous-Paleogene mantle-derived basalts [Sobel, 1995]. The lack of both Cenozoic basalts and seismic velocity anomalies suggests that the thermal effect on surface elevation may not have been important in the Chinese Tian Shan. We thus neglect the U_{therm} term in our analysis.

Because no normal faulting of Cenozoic age has been reported in the Tian Shan, we consider the change in elevation of the Tian Shan purely due to crustal shortening and denudation caused by erosion (Figures 11). Assuming isostatic equilibrium, uniform shortening of the lithosphere, and conservation of mass, the paleoelevation ($e1$) may be related to the present elevation ($e2$), the densities of the crust (ρ_c), mantle lithosphere (ρ_{ml}), and the mantle asthenosphere (ρ_{ma}) as follows:

$$e1 = [(pml - \rho_c)/Sv\rho_{ma}] \{ (\rho_{ml} - \rho_c)(e2 + D + Tc + rc2 - TcSv) + (\rho_{ma} - pml)\{T_L(1 - Sv) + e2 + D + [e2\rho_c - rc2(pml - \rho_c)]/(\rho_{ma} - pml)\} \} \quad (3)$$

where $rc2$ is the present length of the crustal root after shortening (it may be determined by seismic studies on the depth of the Moho), Tc is the thickness of continental crust when its surface is at sea level (~ 35 km), T_L is the thickness of the continental lithosphere when its surface is at sea level (~ 100 km), Sv is stretching strain (final length versus original length) in the vertical direction (it may be determined by the observed horizontal shortening strain), and D is the magnitude of denudation during lithospheric shortening (it may be determined by thermochronological analysis). The vertical stretching strain is inversely proportional to the horizontal shortening strain, that is, $Sv = 1/Sh$. Detailed derivation of (3) is shown in the appendix. It is valid only if (1) isostatic compensation follows Airy isostasy, (2) crustal shortening strain is vertically uniform in a pure-shear fashion, and (3) rate of thermal relaxation is much slower than that of vertical stretching due to horizontal shortening, so that the lithospheric root develops as a result of compression. Under these assumptions, (3) allows evaluation of elevation histories from point to point in a mountain belt.

The present Tian Shan consists of parallel ranges and intermontane basins. We may speculate that the basins have experienced little or no crustal shortening in the Cenozoic and thus remain at low elevations to receive sediments. In contrast, the ranges have been produced by crustal shortening, and their elevations have been modified by erosion. The average elevation of the southern Tian Shan directly north of the Kuche thrust system is between 2000 and 4000 m (Figure 1b). If the south-

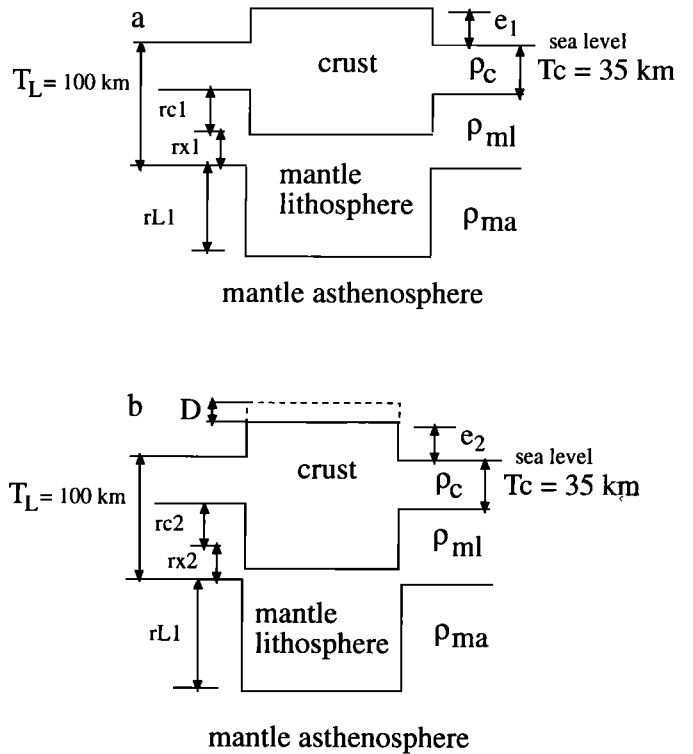


Figure 11. Schematic diagram showing the relationship (a) before and (b) after lithospheric shortening and parameters used to calculate surface uplift of the Tian Shan in the late Cenozoic.

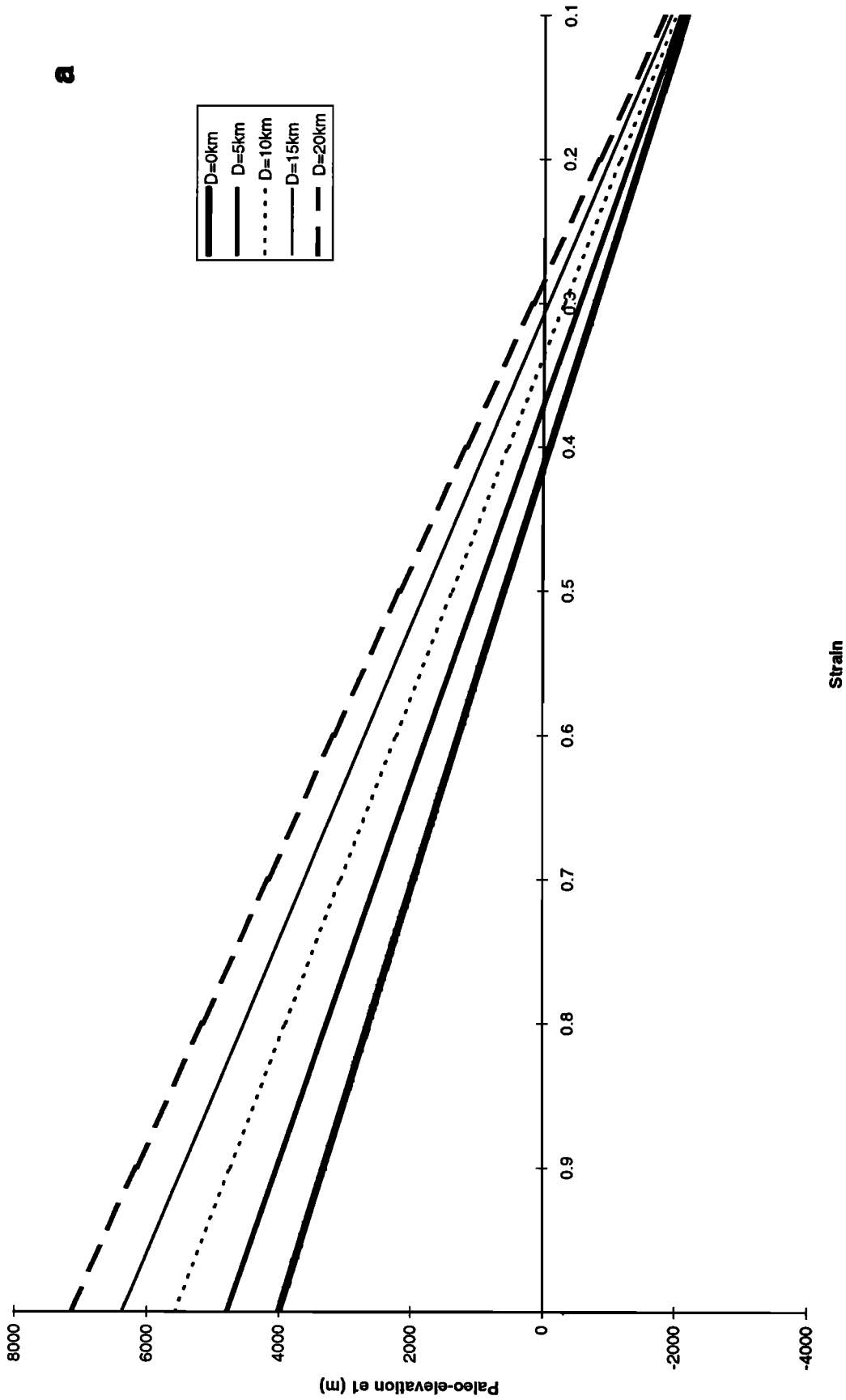


Figure 12. Relationship between paleoelevation (prior to shortening) and shortening strain as a function of denudation. (a) The current Tian Shan elevation is assumed to be 4 km ($T_c = 35$ km). (b) The current elevation is assumed to be 2 km ($T_c = 35$ km). Parameters used in the calculation are $\rho_c = 2.8 \text{ g cm}^{-3}$, $\rho_{ma} = 3.15 \text{ g cm}^{-3}$, $\rho_{ml} = 3.3 \text{ g cm}^{-3}$, $T_c = 35$ km, $T_L = 100$ km, and $r_c = 5$ km. Horizontal shortening strain is defined by present length versus original length.

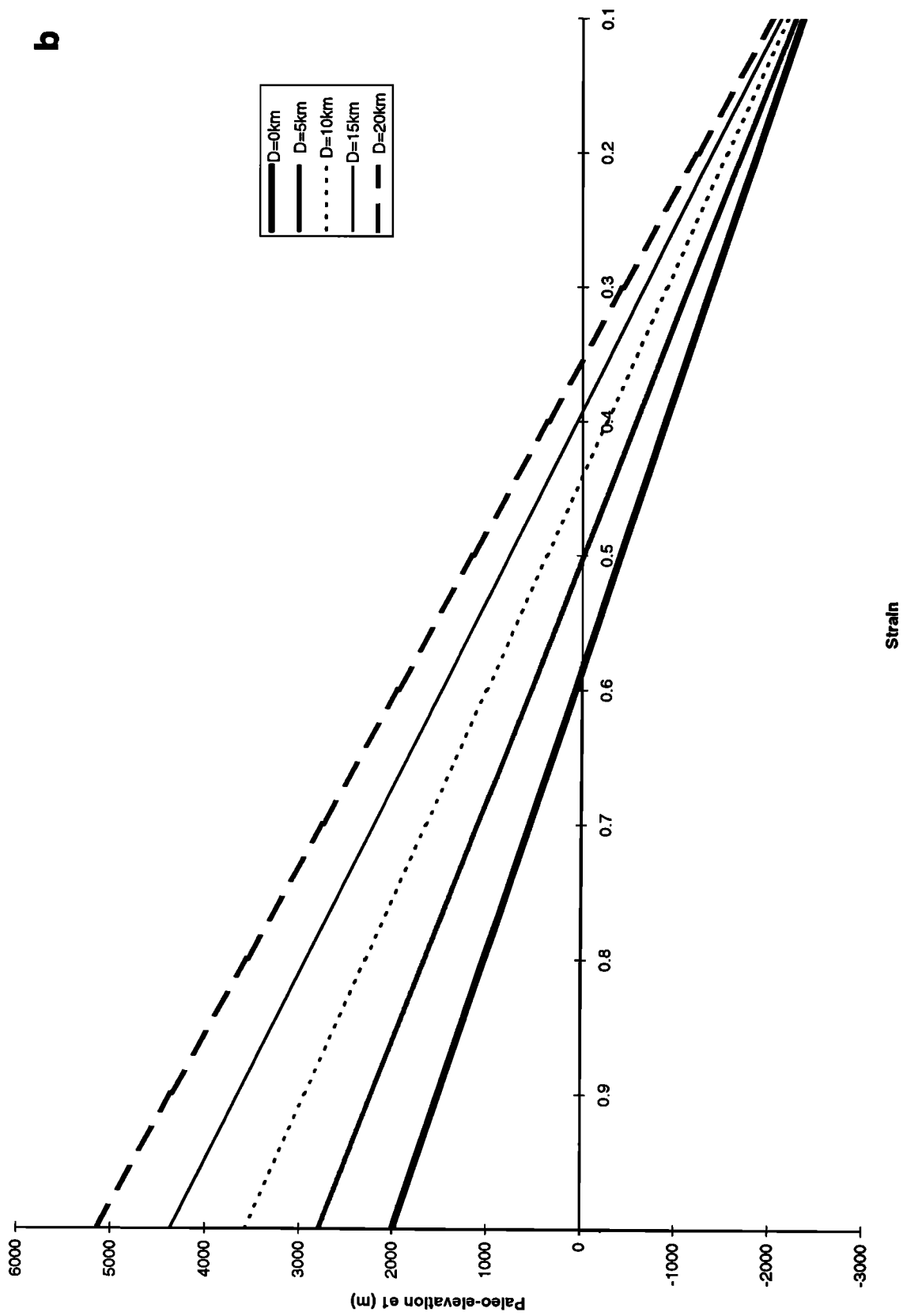


Figure 12. (continued)

ern Tian Shan has experienced the same amount of Cenozoic shortening strain in the southern Tian Shan thrust belt and if 5-km denudation is representative for the high country as indicated by the apatite fission track data of *Hendrix et al.* [1994] and *Sobel and Dumitru* [1997], we may estimate the elevation prior to Cenozoic deformation (Figure 12). We first convert our estimates of shortening strain $\epsilon = (l_f - l_o)/l_o = -20\text{-}30\%$ to horizontal stretch strain, $Sh = l_f/l_o = \epsilon + 1 = 70\text{-}80\%$, where l_o is the original length of a marker bed and l_f is the final length of the marker bed after horizontal shortening. Assuming that the present elevation of the northern part of the southern Chinese Tian Shan is between 2 and 4 km (i.e., $e_2 = 2\text{-}4$ km) and 5-km denudation and 20-30% shortening strain are applied uniformly in the region, that would place its paleoelevation between 1.1 and 3.7 km (Figures 12a and 12b). Taking these estimates at a face value, it implies that the southern Chinese Tian Shan had a significant elevation, between 1.1 and 3.7 km, prior to the initiation of Cenozoic thrusting and that the mountain range has been uplifted between 0.9 and 1.3 km since the early Miocene.

8. Conclusions

Cenozoic deformation of the southern Chinese Tian Shan is expressed by the development of a coherent south verging thrust belt. The western part (the Kashi-Aksu system) is characterized by the occurrence of thin-skin imbricate thrusts which consistently juxtapose the lower Paleozoic strata over the Neogene strata. The central part is expressed by a major thrust (the Kuche thrust) and an oblique thrust ramp (the Korla transfer zone). The former puts middle Paleozoic strata over the Neogene and Quaternary strata, whereas the latter juxtaposes Precambrian crystalline rocks against the Neogene strata. The eastern part consists of widely spaced thrusts involving basement rocks. Geologic mapping and cross-section construction suggest 20-40 km of crustal shortening has occurred in the southern Chinese Tian Shan during the Cenozoic. These are minimum estimates due to both conservative extrapolation of thrust geometries and the location of the hanging wall ramps, which are now largely eroded away, and partial coverage of the thrust belt by the cross sections. The horizontal shortening strain is estimated to be 20-30%.

Thrusting in the southern Chinese Tian Shan may have initiated at 21-24 Ma, as indicated by a facies transition between lacustrine and braided-fluvial sequences in the Kuche foreland basin. Its timing is constrained, in general, by the biostratigraphy and in detail by the magnetostratigraphic investigation. This estimate represents only a minimum age, as the thrusts in the southern Chinese Tian Shan may have propagated southward, and the record we observed only represents the southernmost and thus the youngest part of the thrust belt. If our estimate of timing for the thrust initiation (21-24 Ma) is correct, using the magnitude of shortening (20-40 km) and shortening strain (20-30%) obtained by construction of balanced cross sections, we estimated the slip and strain rates in the southern Chinese Tian Shan thrust belt as 1-1.9 mm yr⁻¹ and 2.9-4.5x10⁻¹⁶ s⁻¹ over the duration of 24-21 m.y., respectively.

Reconnaissance ⁴⁰Ar/³⁹Ar thermochronological analysis together with earlier published apatite fission track analysis suggests that the overall Cenozoic denudation in the Chinese Tian Shan is no more than 10 km and most likely less than 5 km. We demonstrate via a simple physical model that when the thermal effect on changes in surface elevation is negligible, determination of spatial distribution and temporal varia-

tion of both horizontal crustal shortening and denudation provides clues to reconstructing the elevation history of the Tian Shan. The loosely constrained estimates of crustal-shortening and denudation magnitudes from this study suggest that the Chinese Tian Shan may have been elevated between 1.0 and 1.5 km since the onset of Cenozoic thrusting in the region in the early Miocene. This estimate is consistent with the current elevations (1.5-2.0 km) of the southernmost Tian Shan foreland where thrusts occurred in the Upper Cretaceous to early Oligocene marine strata along the south flank of the Chinese Tian Shan.

Appendix

Isostatic equilibrium of the lithospheric section with an elevation e_1 , crustal root rc_1 , and lithospheric root r_{L1} should satisfy the following relation:

$$e_1 = [(\rho_{ml} - \rho_c)rc_1 + r_{L1}(\rho_{ma} - \rho_{ml})]/\rho_c \quad (A1)$$

In the same fashion, the elevation of mountain range after shortening (Sh) and denudation (D) (Figure 11) should satisfy the following relation

$$e_2 = [(\rho_{ml} - \rho_c)rc_2 + r_{L2}(\rho_{ma} - \rho_{ml})]/\rho_c \quad (A2)$$

Conservation of crustal and mantle mass requires

$$(r_{c1} + T_c + e_1)S_v = (r_{c2} + e_2 + D + T_c) \quad (A3)$$

$$(r_{x1} + r_{L1})S_v = (r_{x2} + r_{L2}) \quad (A4)$$

where S_v is the vertical stretching and is equal to $(1/Sh)$. We also note the following geometrical relationships as shown in Figure 12:

$$T_L = T_c + r_{c1} + r_{x1} \quad (A5)$$

$$T_L = T_c + r_{c2} + r_{x2} \quad (A6)$$

Substituting (A2) to (A6), we obtain the following relationship:

$$e_1 = [(\rho_{ml} - \rho_c)/S_v \rho_{ma}] \{ (\rho_{ml} - \rho_c)(e_2 + D + T_c + r_{c2} - T_c S_v) + (\rho_{ma} - \rho_{ml}) \{ T_L(1 - S_v) + e_2 + D + [e_2 \rho_c - r_{c2}(\rho_{ml} - \rho_c)] / (\rho_{ma} - \rho_{ml}) \} \} \quad (A7)$$

In our calculation, we assumed that $T_c = 35$ km, $T_L = 100$ km, $rc_2 = 10$ km, $\rho_c = 2.8$ g cm⁻³, $\rho_{ml} = 3.3$ g cm⁻³, and $\rho_{ma} = 3.2$ g cm⁻³. Parameters such as D , S_v , e_2 , rc_2 are derived from observations in the Tian Shan region.

Acknowledgments. This research was supported by a NSF grant EA-9220105 awarded to A. Yin and S. Nie and by a grant from IGPP of the Lawrence Livermore National Laboratory awarded to F.J. Ryerson and A. Yin. Joe Kirschvink is especially thanked for generously providing his paleomagnetic laboratory for our magnetostratigraphic analysis. We are grateful to Peter Rumelhart for discussions of the Tian Shan geology and assistance in drafting some of the figures. Peter Molnar read an early version of the paper and provided many valuable comments on improving both its text and content. We thank Doug Burbank, Steve Graham, and Ed Sobel for providing constructive, thorough, and critical reviews. Their comments have led to significant reorganization and improvement of the original manuscript.

References

- Abdrakhmatov, K. Y., et al., Relative recent construction of the Tien Shan inferred from GPS measurements of present-day crustal deformation rates, *Nature*, **384**, 450-453, 1996.
- Allen, M. B., B. F. Windley, C. Zhang, Z. Zhao, and G. Wang, Basin evolution within and adjacent to the Tien Shan range, NW China, *J. Geol. Soc. London*, **148**, 369-378, 1991.
- Allen, M. B., B. F. Windley, and C. Zhang, Cenozoic tectonics in the Urumqi-Korla region of the Chinese Tien Shan, *Geol. Rundsch.*, **83**, 406-416, 1992.
- Allen, M. B., B. F. Windley, and C. Zhang, Paleozoic collisional tectonics and magmatism of the Chinese Tien Shan, central Asia, *Tectonophysics*, **220**, 89-115, 1993.
- Amano, K., and A. Taira, Two-phase uplift of high Himalayas since 17 Ma, *Geology*, **20**, 391-394, 1992.
- Avouac, J.-P., and G. Peltzer, Active tectonics in southern Xinjiang, China: Analysis of terrace and normal fault scarp degradation along the Hotan-Qira fault system, *J. Geophys. Res.*, **98**, 21,773-21,803, 1993.
- Avouac, J. P., P. Tapponnier, M. Bai, H. You, and G. Wang, Active thrusting and folding along the northern Tien Shan and late Cenozoic rotation of the Tarim relative to Dzungaria and Kazakhstan, *J. Geophys. Res.*, **98**, 6755-6804, 1993.
- Blatt, H., G. Middleton, and R. Murray, *Origin of Sedimentary Rocks*, 782 pp., Prentice-Hall, Englewood Cliffs, N. J., 1980.
- Burbank, D. W., and G. D. Johnson, The late Cenozoic chronological and stratigraphic development of the Kashmir intermontane basin, northwestern Himalaya, *Palaeogeogr. Palaeoclimatol. Palaeoecol.*, **43**, 205-235, 1983.
- Burbank, D. W., J. Verges, J. A. Munoz, and P. Bentham, Coeval hindward- and forward-imbicating thrusting in the south-central Pyrenees, Spain: Timing and rates of shortening and deposition, *Geol. Soc. Am. Bull.*, **104**, 3-17, 1992.
- Burbank, D. W., R. A. Beck, and T. Mulder, The Himalayan foreland basin, in *Tectonic Evolution of Asia*, edited by A. Yin and T. M. Harrison, pp. 149-190, Cambridge Univ Press, New York, 1996.
- Burchfiel, B. C., and L. H. Royden, Tectonics of Asia 50 years after the death of Emile Argand, *Eclogae Geol. Helv.*, **84**, 599-629, 1991.
- Burchfiel, B. C., P. Zhang, Y. Wang, W. Zhang, F. Song, Q. Deng, P. Molnar, and L. Royden, Geology of the Haiyuan fault zone, Ningxia-Hui autonomous region, China, and its relation to the evolution of the northeastern margin of the Tibetan Plateau, *Tectonics*, **10**, 1091-1110, 1991.
- Burchfiel, B. C., P. Molnar, Q. Deng, Z. Wu, X. Feng, J. Li, and H. You, Latest Cenozoic rates of shortening across the margins of Tien Shan, Xinjiang, China, *Geol. Soc. Am. Abstr. Programs*, **26**, 462, 1994.
- Burov, M. C., Kogan, H. Lyon-Caen, and P. Molnar, Gravity anomalies, the deep structure, and dynamic processes beneath the Tien Shan, *Earth Planet. Sci. Lett.*, **96**, 367-383, 1990.
- Burtman, V. S., and P. Molnar, Geological and geophysical evidence for deep subduction of continental crust beneath the Parur, *Spec. Pap. Geol. Soc. Am.*, **281**, 1-76, 1993.
- Butler, R. F., *Paleomagnetism: Magnetic Domains to Geologic Terranes*, 319 pp., Blackwell Sci., Cambridge, Mass., 1992.
- Cande, S. C., and D. V. Kent, A new geomagnetic polarity timescale for the late Cretaceous and Cenozoic, *J. Geophys. Res.*, **97**, 13,917-13,951, 1992.
- Carroll, A. R., S. A. Graham, M. S. Hendrix, D. Ying, and D. Shou, Late Paleozoic tectonic amalgamation of northwestern China: Sedimentary record of the northern Tarim, northwestern Turpan, and southern Junggar basins, *Geol. Soc. Am. Bull.*, **107**, 571-594, 1995.
- Chen, Z., Geologic map of Xinjiang Uygur autonomous region, China, 4 sheets, 1:2,000,000, scale, Geol. Publ. House, Beijing, China, 1985.
- Coleman, R. G., Continental growth of northwest China, *Tectonics*, **8**, 621-636, 1989.
- Cox, A., A stochastic approach towards understanding the frequency and polarity bias of geomagnetic reversals, *Phys. Earth Planet. Inter.*, **24**, 178-190, 1981.
- Craig, P. A., Cenozoic development of the Kuche Foreland of the Tarim Basin, Xinjiang, China, 198 pp., M. S. thesis, Univ. of Calif., Los Angeles, 1995.
- Dewey, J. F., and K. Burke, Tibetan, Variscan and Precambrian basement reactivation: Products of continental collision, *J. Geol.*, **81**, 683-692, 1973.
- England, P., and G. Houseman, The mechanics of the Tibetan plateau, *Philos. Trans. R. Soc. London, ser. A*, **326**, 301-320, 1988.
- Fisher, R. A., Dispersion on a sphere, *Proc. R. Soc. London*, **A217**, 295-305, 1953.
- Hao, Y. C., and X. L. Zeng, Discussion of the Mesozoic-Cenozoic evolution of the western Tarim basin based on foraminifera, *Chin. Micropaleontol. Bull.*, **1**, 1-4, 1984.
- Hao, Y. C., X. L. Zeng, S. Y. Qiu, and X. X. He, Miocene foraminifera of the Tarim basin, Xinjiang and their geological significance, *Bull. Chin. Acad. Geol. Sci.*, **4**, 69-79, 1982.
- Haq, B. U., J. Hardenbol, and P. R. Vail, Chronology of fluctuating sea levels since the Triassic, *Science*, **235**, 1156-1167, 1987.
- Harrison, T. M., P. Copeland, W. S. F. Kidd, and A. Yin, Raising Tibet, *Science*, **255**, 1663-1670, 1992a.
- Harrison, T. M., W. Chen, P. H. Leloup, F. J. Ryerson, and P. Tapponnier, An early Miocene Transition in deformation regime within the Red River fault zone, Yunnan, and its significance for Indo-Asian tectonics, *J. Geophys. Res.*, **97**, 7159-7182, 1992b.
- Harrison, T. M., P. Copeland, S. A. Hall, J. Quade, S. Burner, T. P. Ojha, and W. S. F. Kidd, Isotopic preservation of Himalayan/Tibetan uplift, denudation, and climate histories of two molasse deposits, *J. Geol.*, **100**, 157-175, 1993.
- Heller, P. L., C. L. Angevine, N. S. Winslow, and C. Paola, Two phase stratigraphic model of foreland basin sequences, *Geology*, **16**, 501-504, 1988.
- Hendrix, M. S., S. A. Graham, A. R. Carroll, E. R. Sobel, C. L. McKnight, B. J. Schuelein, and Z. X. Wang, Sedimentary record and climatic implications of recurrent deformation in the Tien Shan. Evidence from Mesozoic strata of the north Tarim, south Junggar, and Turpan basins, northwest China, *Geol. Soc. Am. Bull.*, **104**, 53-79, 1992.
- Hendrix, M. S., T. A. Dumitru, and S. A. Graham, Late Oligocene-early Miocene unroofing in the Chinese Tien Shan: An early effect of the India-Asia collision, *Geology*, **22**, 487-490, 1994.
- Huang, T. K., On Major Tectonic Forms of China, *Geol. Soc. China Mem. ser. A*, **20**, 165 pp., 1945.
- Jia, C., H. Yao, G. Wei, and L. Wei, Plate tectonic evolution and characteristics of major tectonic units of the Tarim basin, in *The Tarim Basin*, edited by X. Tong and D. Liang, pp. 207-225, Xinjiang Sci., Urumqi, China, 1991.
- Johnson, N. M., and V. E. McGee, Magnetic polarity stratigraphy: Stochastic properties of data, sampling problems, and the evaluation of interpretations, *J. Geophys. Res.*, **88**, 1213-1221, 1983.
- Johnson, N. M., K. A. Sheikh, E. Dawson-Saunders, and L. E. McRae, The use of magnetic-reversal time lines in stratigraphic analysis: a case study measuring variability in sedimentation rates, in *New Perspectives in Basin Analysis* edited by K. L. Kleinspehn and C. Paola, pp. 189-200, Springer-Verlag, New York, 1988.
- Jordan, T. E., P. B. Flemings, and J. A. Beer, Dating thrust-fault activity by use of foreland-basin strata, in *New Perspectives in Basin Analysis*, edited by K. L. Kleinspehn and C. Paola, pp. 307-330, Springer-Verlag, New York, 1988.
- Kang Y., *Characteristics of Petroleum Geology and Resource Assessment of the Tarim Basin, China*, 348 pp., Geologic Publishing House, Beijing, 1996.
- Kosarev, G. L., N. V. Petersen, L. P. Vinnik, and S. W. Roecker, Receiver functions for the Tien Shan analog broadband network. Contrasts in the evolution of structures across the Talasso-Fergana fault, *J. Geophys. Res.*, **98**, 4437-4448, 1993.
- Leloup, P. H., T. M. Harrison, F. J. Ryerson, Chen Wenji, Li Qi, P. Tapponnier, and R. Lacassin, Structural, petrological, thermal evolution of a Tertiary ductile strike-slip shear zone, Diancan Shan (Yunnan, PRC), *J. Geophys. Res.*, **98**, 6715-6743, 1993.
- Li, D., D. Liang, C. Jia, G. Wang, Q. Wu, and D. He, Hydrocarbon accumulations in the Tarim basin, China, *AAPG. Bull.*, **80**, 1587-1603, 1996.
- Liu, H., H. Laing, L. Cai, Y. Xia, and L. Liu, Evolution and structural style of Tianshan and adjacent basins, northwestern China, *J. China Univ. Geosci.*, **5**, 46-54, 1994.
- Lü H., and Q. Luo, *Algeas in the Tarim Basin*, 113 pp., Chin. Sci. Technol., Beijing, 1990.
- Lu, H., D. Howell, D. Jia, D. Cai, S. Wu, C. Chen, Y. Shi, and Z. C. Valin, Rejuvenation of the Kuqa foreland basin, northern flank of the Tarim basin, northwestern China, *Int. Geol. Rev.*, **36**, 1151-1158, 1994.
- Lyon-Caen, H., and P. Molnar, Gravity anomalies and the structure of western Tibet and the southern Tarim basin, *Geophys. Res. Lett.*, **11**, 1251-1254, 1984.
- Makeyeva, L. L., L. P. Vinnik, and S. W. Roecker, Shear wave splitting and small-scale convection in the continental upper mantle, *Nature*, **358**, 144-147, 1992.
- McDougall, I., and T. M. Harrison, *Geochronology and thermochronology by the ⁴⁰Ar/³⁹Ar Method*, 212 pp., Oxford Univ. Press, New York, 1988.
- McElhinny, M. W., *Paleomagnetism and Plate Tectonics*, 356 pp., Cambridge Univ. Press, New York, 1973.
- McKnight, C. L., Structural styles and tectonic significance of Tien Shan foothill fold and thrust belts, northwest China, Ph.D. thesis, 207 pp., Stanford Univ., Stanford, Calif., 1993.
- McKnight, C. L., Compressional episodes, structural styles, and shortening estimates, southern Tien Shan foreland, NW China, *Geol. Soc. Am. Abstr. Programs*, **26**, 463, 1994.
- Molnar, P., and P. Tapponnier, Cenozoic tectonics of Asia: Effects of a continental collision, *Science*, **189**, 419-426, 1975.
- Molnar, P., P. England, and J. Martinod, Mantle dynamics, the uplift of the Tibetan plateau, and the Indian monsoon, *Rev. Geophys.*, **31**, 357-396, 1993.
- Molnar, P., et al., Quaternary climate change and the formation of river terrace across growing anticlines on the northern flank of the Tien Shan, China, *J. Geol.*, **102**, 583-602, 1994.
- Nie, S., A. Yin, P. A. Craig, G. Yang, and X. Qian, Tertiary structural evolution of the Kuche thrust system in the southern Tien Shan region, *Geol. Soc. Am. Abstr. Programs*, **26**, 463, 1994.
- Norin, E., Geologic reconnaissances in the Chinese Tien Shan: Reports from the scientific expedition to the north-western provinces of China under the leadership of Dr. Sven Hedin, *Sino-Swed. exped. publ.*, **16**, 229 pp., Sino-Swed. Exped., Stockholm, 1941.
- Pan, H., Late Cretaceous-Early Tertiary marine gastropod fossils from the western Tarim basin (in Chinese with English abstract), *Xinjiang Stratigraphic Research Series*, **4**, pp. 1-100, Xinjiang Bur. of Geol. and Miner. Resour., Urumqi, China, 1990.
- Peltzer, G., and P. Tapponnier, Formation and evolution of strike-slip faults, rifts, and basins during the India-Asia collision. An experimental approach, *J. Geophys. Res.*, **93**, 15,085-15,117, 1988.
- Roecker, S. W., T. M. Sabitova, L. P. Vinnik, Y. A. Burmakov, M. I. Golvanov, R. Mamatkanova, and L. Munirova, Three-dimensional elastic wave velocity structure of the western and central Tien Shan, *J. Geophys. Res.*, **98**, 15,779-15,795, 1993.
- Ruddiman, W. F., and J. E. Kutzbach, Forcing of Late Cenozoic northern hemisphere climate by plateau uplift in southern Asia and the American west, *J. Geophys. Res.*, **94**, 18,409-18,427, 1989.
- Sadler, P. M., Sediment accumulation rates and the completeness of stratigraphic sections, *J. Geol.*, **89**, 569-584, 1981.
- Smith, R. B., Formation of folds, boudinage, and

- mullions in non-Newtonian materials, *Geol. Soc. Am. Bull.*, 88, 312-320, 1977.
- Sobel, E. R., Basin analysis and apatite fission-track thermochronology of the Jurassic-Paleogene southwestern Tarim Basin, NW China, Ph.D thesis, 308 pp., Stanford Univ., Stanford, Calif., 1995.
- Sobel, E. R., and T. A. Dumitru, Thrusting and exhumation around the margins of the western Tarim basin during the India-Asia collision, *J. Geophys. Res.*, 102, 5043-5063, 1997.
- Sun, D., Late Cretaceous brachiopods from the western Tarim basin, south Xinjiang, China (in Chinese with English abstract), *Xinjiang Stratigraphic Res. Ser.* 4, 133-149 pp., Xinjiang Bur. of Geol. and Miner. Resour., Urumqi, China, 1991.
- Suppe, J., T. T. Chou, and C. H. Stephen, Rate of folding and faulting determined from growth strata, in *Thrust Tectonics* edited by K. R. McClay, pp. 105-122, Chapman and Hall, New York, 1992.
- Tang, T., Y. Xue, and C. Yu, Characteristics and sedimentary environments of the Late Cretaceous to Early Tertiary marine strata in the western Tarim basin, China (in Chinese with English abstracts), *Xinjiang Stratigraphic Res. Ser.* 9, 1-138 pp., Xinjiang Bur. of Geol. and Miner. Resour., Urumqi, China, 1992.
- Tapponnier, P., R. Lacassin, P. H. Leloup, U. Sharer, D. Zhong, X. Liu, S. Ji, L. Zhang, and J. Zhong, The Ailao Shan/Red River metamorphic belt: Tertiary left-lateral shear between Indochina and South China, *Nature*, 343, 431-437, 1990.
- Tapponnier, P., and P. Molnar, Active faulting and Cenozoic tectonics of the Tien Shan, Mongolia, and Baikal regions, *J. Geophys. Res.*, 84, 3425-3459, 1979.
- Tapponnier, P., G. Peltzer, A. Y. Le Dain, R. Armijo, and P. Cobbold, Propagating extrusion tectonics in Asia, *Geology*, 10, 611-616, 1982.
- Windley, B. F., M. B. Allen, C. Zhang, Z. Y. Zhao, and G. R. Wang, Paleozoic accretion and Cenozoic reformation of the Chinese Tien Shan Range, central Asia, *Geology*, 18, 128-131, 1990.
- Xinjiang Bureau of Geology and Mineral Resources (Xinjiang BGM), Geologic map of the Kashi region, scale 1:1,000,000, Chin. Minist. Geol. and Miner. Resour., Beijing, 1965a.
- Xinjiang Bureau of Geology and Mineral Resources (Xinjiang BGM), Geologic map of the Zhanbale region, scale 1:200,000, Chin. Minist. of Geol. and Miner. Resour., Beijing, 1965b.
- Xinjiang Bureau of Geology and Mineral Resources (Xinjiang BGM), Geologic map of the Akeqi region, scale 1:200,000, Chin. Minist. of Geol. and Miner. Resour., Beijing, 1966a.
- Xinjiang Bureau of Geology and Mineral Resources (Xinjiang BGM), Geologic map of the Subashi region, scale 1:200,000, Chin. Minist. of Geol. and Miner. Resour., Beijing, 1966b.
- Xinjiang Bureau of Geology and Mineral Resources (Xinjiang BGM), Geologic map of the Kuche region (1:200,000), Chin. Minist. of Geol. and Miner. Resour., Beijing, 1966c.
- Xinjiang Bureau of Geology and Mineral Resources (Xinjiang BGM), Geologic map of the Wushi region, scale 1:200,000, Chin. Minist. of Geol. and Miner. Resour., Beijing, 1967.
- Xinjiang Bureau of Geology and Mineral Resources (Xinjiang BGM), Geologic map of the Kule region, scale 1:200,000, Chin. Minist. of Geol. and Miner. Resour., Beijing, 1975.
- Xinjiang Bureau of Geology and Mineral Resources (Xinjiang BGM), Stratigraphy of Xinjiang, Chin. Geol., Beijing, 1981.
- Xinjiang Bureau of Geology and Mineral Resources (Xinjiang BGM), *Regional Geology of Xinjiang* (in Chinese with English Abstract), 841 pp., 1992.
- Xinjiang Institute of Geography, Academia Sinica, *The Evolution of the Tian Shan* (in Chinese), 188 pp., Sci. Press, Beijing, 1986.
- Xinjiang Regional Mapping Team, *The Geology of Granitoids in the Tian Shan*, 247 pp., Xinjiang Bureau of Geol. and Miner. Resour., Urumqi, China, 1985.
- Yan, L., Three important structural patterns in the Tarim basin: "Y"-shaped fault systems, hanging wall anticlines, and anticlines, in *The Tarim Basin* edited by X. Tong and D. Liang, pp. 195-206. Xinjiang Sci., Urumqi, China, 1991.
- Yang, H., X. Jaing, and S. Lin, Late Cretaceous-early Tertiary ostracod fauna from western Tarim basin, South Xinjiang, China 1995 (in Chinese with English abstract), *Xinjiang Stratigraphic Research Series* 7, 1-173 pp., Xinjiang Bur. of Geol. and Miner. Resour., Urumqi, China, 1995.
- Yang, S., Late Cretaceous and Early Tertiary echinoids from the Tarim basin (in Chinese with English abstract), *Xinjiang Stratigraphic Research Series* 4, 101-132 pp., Xinjiang Bur. of Geol. and Miner. Resour., Urumqi, China, 1991.
- Ye, C. H., and R. J. Huang, Tertiary stratigraphy of the Tarim Basin, in *Stratigraphy of the Tarim Basin*, edited by Z. Zhou and P. Chen, pp. 308-363, Sci. Press, Beijing, 1990.
- Yin, A., and S. Nie, A Phanerozoic palinspastic reconstruction of China and its neighboring regions, in *Tectonic Evolution of Asia*, edited by A. Yin and T. M. Harrison, pp. 442-485, Cambridge Univ. Press, New York, 1996.
- Yin, A., and G. Oertel, Kinematics and strain distribution of a thrust-related fold system in the Lewis thrust plate, northwestern Montana (U.S.A.), *J. Struct. Geol.*, 15, 707-719, 1993.
- Yin, A., T. M. Harrison, F. J. Ryerson, W. J. Chen, W. S. F. Kidd, and P. Copeland, Tertiary structural evolution of the Gangdese thrust system in southeastern Tibet, *J. Geophys. Res.*, 99, 18,175-18,201, 1994.
- Zhang, P., B. C. Burchfiel, P. Molnar, W. Zhang, D. Jiao, Q. Deng, Y. Wang, L. Royden, and F. Song, Amount and style of late Cenozoic deformation in the Liupan Shan area, Ningxia autonomous region, China, *Tectonics*, 10, 1111-1129, 1991.
- Zhang, Y. M., Z. R. Wang, and G. Z. He, Analyses of geologic feature and potash salt genesis condition in Kuche basin, Xinjiang, China, *Xinjiang Geol.*, 4, 57-71, 1986.
- Zhong, S., Calcareous nannofossils from the Upper Cretaceous and lower Tertiary in the western Tarim Basin, south Xinjiang, China (in Chinese with English abstract), *Xinjiang Stratigraphic Research Series* 5, 1-121 pp., Xinjiang Bur. of Geol. and Miner. Resour., Urumqi, China, 1992.
- Zhou, D., T. A. Dumitru, S. A. Graham, and M. S. Hendrix, Apatite fission-track record of Mesozoic and Cenozoic episodic reactivation of the Chinese Tien Shan, *Geol. Soc. Am. Abstr. Programs*, 27, 456, 1995.
- Zhou, Q., and J. Zheng, *Structural Analysis of the Tarim Basin* (in Chinese), 144 pp., Sci. Press, 1990.
- Zhou, Z., and P. Chen, *Paleontology, Stratigraphy, and Geologic Evolution of the Tarim Basin* (in Chinese), 336 pp., Sci. Press, Beijing, 1990.

P. Craig, Shell Deepwater Production, Inc., P. O. Box 60834, New Orleans, LA 70160 (e-mail: pcraig@shellus.com)

T.M. Harrison and A. Yin, Department of Earth and Space Sciences and Institute of Geophysics and Planetary Physics, University of California, Los Angeles, CA 90095-1567. (e-mail: yin@ess.ucla.edu)

S. Nie, Petroconsultants, P. O. Box 152, 24 Chemin de la Mairie, 1258 Perly-Geneva, Switzerland (e-mail: shangyou.nie@petroconsultants.com)

X. Qiang, Department of Geology, Peking University, Beijing 100871, People's Republic of China.

F.J. Ryerson, Institute of Geophysics and Planetary Physics, Lawrence Livermore National Laboratory, Livermore, CA 95440. (e-mail: ryer-son1@popeye.llnl.gov)

(Received May 15, 1997;
revised September 11, 1997,
accepted November 4, 1997.)